Distribution of Neurotransmitter Receptors and Zinc in the Pigeon (*Columba livia*) Hippocampal Formation: A Basis for Further Comparison With the Mammalian Hippocampus

Christina Herold,[1]* Verner P. Bingman,[2] Felix Ströckens,[3] Sara Letzner,[3] Magdalena Sauvage,[4] Nicola Palomero-Gallagher,[5] Karl Zilles,[5,6] and Onur Güntürkün[3]

[1]C. & O. Vogt Institute of Brain Research, University of Düsseldorf, 40225 Düsseldorf, Germany
[2]Department of Psychology and J.P. Scott Center for Neuroscience, Bowling Green State University, Bowling Green, Ohio 43403
[3]Department of Biopsychology, Institute of Cognitive Neuroscience, Faculty of Psychology, Ruhr-University Bochum, 44780 Bochum, Germany
[4]Research Department of Neuroscience, Mercator Research Group "Structure of Memory," Faculty of Medicine, Ruhr-University Bochum, 44780 Bochum, Germany
[5]Institute of Neuroscience and Medicine INM-1, Research Center Jülich, 52425 Jülich, Germany
[6]Department of Psychiatry, Psychotherapy and Psychosomatics, RWTH Aachen University, and JARA–Translational Brain Medicine, 52074 Aachen, Germany

ABSTRACT

The avian hippocampal formation (HF) and mammalian hippocampus share a similar functional role in spatial cognition, but the underlying neuronal mechanisms allowing the functional similarity are incompletely understood. To understand better the organization of the avian HF and its transmitter receptors, we analyzed binding site densities for glutamatergic AMPA, NMDA, and kainate receptors; $GABA_A$ receptors; muscarinic M_1, M_2 and nicotinic (nACh) acetylcholine receptors; noradrenergic α_1 and α_2 receptors; serotonergic 5-HT_{1A} receptors; dopaminergic $D_{1/5}$ receptors by using quantitative in vitro receptor autoradiography. Additionally, we performed a modified Timm staining procedure to label zinc. The regionally different receptor densities mapped well onto seven HF subdivisions previously described. Several differences in receptor expression highlighted distinct HF subdivisions. Notable examples include 1) high $GABA_A$ and α_1 receptor expression, which rendered distinctive ventral subdivisions; 2) high α_2 receptor expression, which rendered distinctive a dorsomedial subdivision; 3) distinct kainate, α_2, and muscarinic receptor densities that rendered distinctive the two dorsolateral subdivisions; and 4) a dorsomedial region characterized by high kainate receptor density. We further observed similarities in receptor binding densities between subdivisions of the avian and mammalian HF. Despite the similarities, we propose that 300 hundred million years of independent evolution has led to a mosaic of similarities and differences in the organization of the avian HF and mammalian hippocampus and that thinking about the avian HF in terms of the strict organization of the mammalian hippocampus is likely insufficient to understand the HF of birds. J. Comp. Neurol. 522:2553–2575, 2014.

INDEXING TERMS: hippocampus; entorhinal cortex; receptor; avian; autoradiography; zinc

In both mammals and birds, the hippocampal formation (HF) plays a similar role in spatial cognition (Colombo and Broadbent, 2000; Bingman et al., 2005) and shows comparable neuroanatomical, neurochemical, and electrophysiological characteristics (Bingman et al., 2005). The overall homology between the mammalian and avian HF is well established (Reiner et al.,

Grant sponsor: Alexander von Humboldt-Stiftung (to V.P.B.); Grant sponsor: HGF Program "Function and Dysfunction of the Nervous System" (to K.Z.); Grant sponsor: Deutsche Forschungsgemeinschaft; Grant number: SFB874 (to O.G.).

*CORRESPONDENCE TO: Christina Herold, C. & O. Vogt Institute of Brain Research, University of Düsseldorf, 40225 Düsseldorf, Germany.
E-mail: christina.herold@uni-duesseldorf.de

Received August 16, 2013; Revised January 17, 2014;
Accepted January 21, 2014.
DOI 10.1002/cne.23549
Published online January 29, 2014 in Wiley Online Library (wileyonlinelibrary.com)

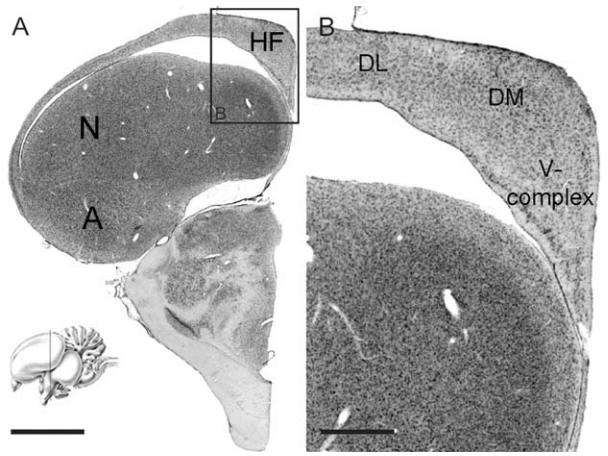

Figure 1. Nissl-stained transverse section of the forebrain of the pigeon. **A:** Full transverse section at atlas level A 6.75 (Karten and Hodos, 1967). The boxed area indicates the region of interest, the hippocampal formation. At bottom, a lateral view of the pigeons brain was prepared that indicates the location of the plane of the illustrated section (not scaled). **B:** Enlarged image of the hippocampal formation labeled in A. A, arcopallium; DM, dorsomedial region of HF; DL, dorsolateral region of HF; HF, hippocampal formation; N, nidopallium; V-complex, region that comprises the ventral subdivisions of the HF. Scale bars = 2.5 mm in A; 500 μm in B.

2004; Jarvis et al., 2013), but what continues to concern researchers is uncertainty with respect to what, if any, areas of the avian HF correspond to the well-defined dentate gyrus (DG) and Ammon's horn (CA3 and CA1 in particular) of the mammalian hippocampus. The avian HF (Fig. 1) can be coarsely divided into ventromedial (V-complex), dorsomedial (DM), and dorsolateral (DL) subdivisions. Further subdivisions (ventromedial Tr, Vl, and Vm; dorsomedial DMd and DMv; and dorsolateral DLd and DLv; Fig. 2) have been described (Erichsen et al., 1991; Kahn et al., 2003; Atoji and Wild, 2004). Erichsen et al. (1991) proposed that the medial (Vm) and lateral (Vl) dense cell layers of the V-complex correspond to areas of Ammon's horn, the area between the two cell layers (Tr) to the hilar region, and the dorsomedial HF (DMd and DMv) to the dentate gyrus (DG). However, they acknowledged uncertainty with respect to a dentate gyrus-like structure in the avian HF. The tracing study of Kahn et al. (2003) and Székély and Krebs (1996) in zebra finch (*Taeniopygia guttata*) essentially led to the same conclusions with respect to the interclass comparisons of Erichsen et al. (1991). By contrast, Atoji and Wild (2004) proposed, based on connectivity data and kainic acid lesions, that the cell layers of the V-complex actually correspond to the DG, whereas an Ammon's horn-like subdivision is found in DM. Timm staining for zinc is a powerful marker for mossy fibers in mammals and has also been used to search for a DG mossy fiber-like system in bird species other than pigeons (Faber et al., 1989; Aboitiz, 1993; Montagnese et al., 1993, 1996; Tömböl et al., 2000b), but those Timm staining studies failed to reveal distinct, rat-like fiber labeling in the HF of birds. However, zinc labeling has been used to classify different types of glutamatergic synapses that can be found numerously in the CA fields (Sindreu et al., 2003).

To understand better the organization of the avian HF and its transmitter receptors and to shed light on the extent to which there are anatomically defined structures in the avian HF that are comparable to the DG and CA regions in the mammalian hippocampus, we mapped the distribution of 11 different neurotransmitter receptors in the pigeon HF. Our goal was to describe the regional receptor expression in the pigeon hippocampal formation as well as to characterize the receptor organization of HF in distinct subdivisions. We then compared the receptor binding data with published data for the hippocampus in different mammalian species (Kraemer et al., 1995; Palomero-Gallagher et al., 2003; Topic et al., 2007; Cremer et al., 2011). To complement the receptor data, we further carried out a zinc-staining procedure in the pigeon.

MATERIALS AND METHODS

Receptor autoradiography

We examined a total of six adult pigeons (*Columba livia*) of unknown sex. Animals were obtained from local breeders and were housed in individual cages (30 × 30 × 45 cm) in a temperature (21°C ± 1°C)- and humidity-controlled room with a 12-hour light/dark circle. The subjects had access to grit, food, and water ad libitum. All experimental procedures were approved by national authorities (LANUV NRW, Germany) and were carried out in accordance with the National Institutes of Health *Guide for care and use of laboratory animals*. Animals were decapitated and the brains removed from the skull, frozen immediately in isopentane at −40°C, and stored at −70°C. Serial coronal 10-μm sections were cut with a cryostat microtome (2800 Frigocut E; Reichert-Jung). Sections were thaw mounted on gelatinized slides, freeze dried, and stained with a modified cell body staining for cytoarchitectonic analysis or processed for receptor autoradiography (Merker, 1983; Palomero-Gallagher et al., 2008).

Details of the autoradiographic labeling procedure have been published elsewhere (Zilles et al., 2002a,b; Schleicher et al., 2005). Binding protocols are summarized in Table 1. Three steps were performed in the following sequence: 1) A preincubation step removed endogenous ligand from the tissue. 2) During the main incubation step, binding sites

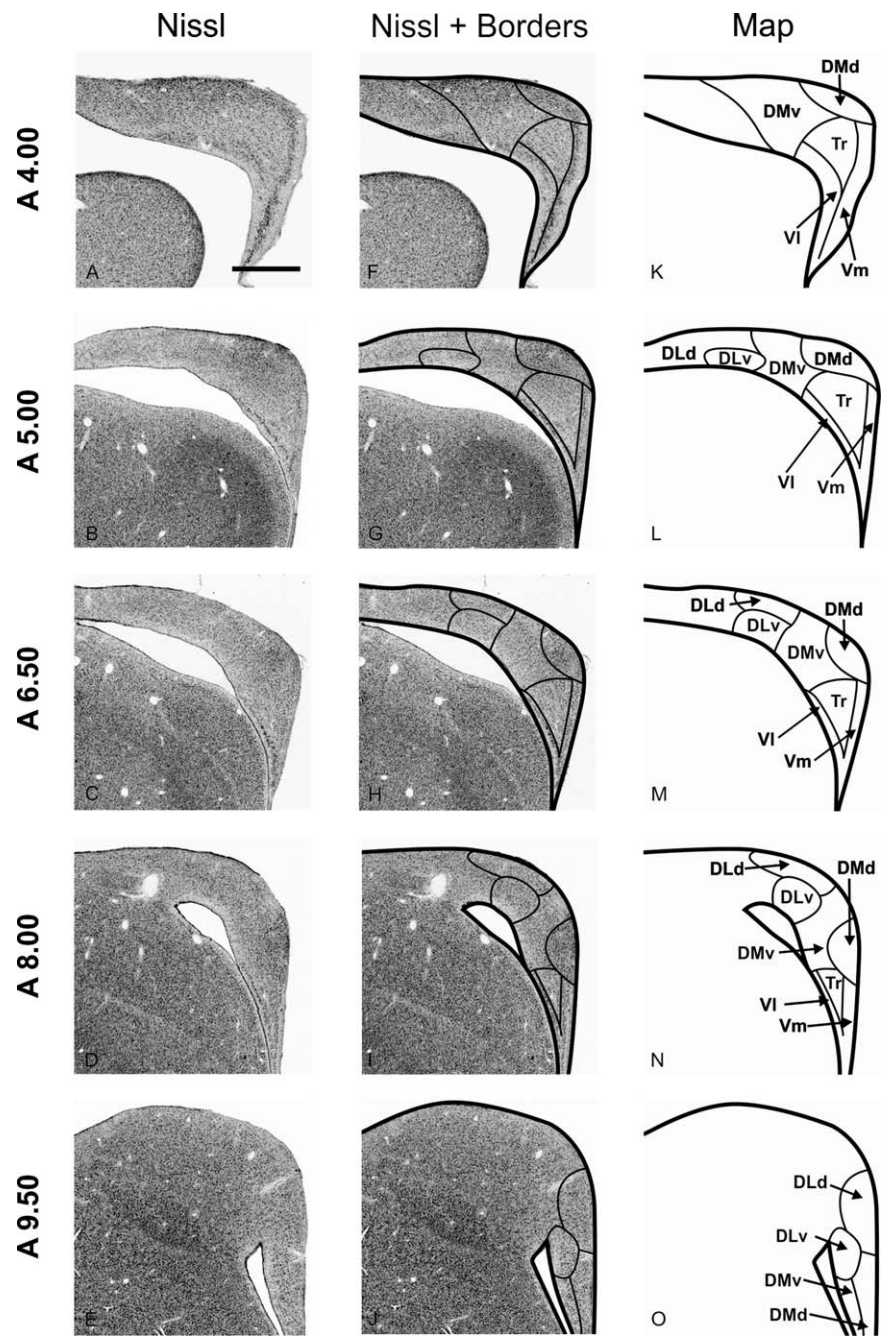

Figure 2. Nissl-stained and schematic representation of the pigeon hippocampal formation subdivision boundaries from rostrocaudal atlas levels A 4.00 to A 9.50 (Karten and Hodos, 1967). **A–E:** Nissl-stained coronal sections of the hippocampal formation. **F–J:** Nissl-stained coronal section with the boundaries following Atoji and Wild (2004, 2006). **K–O:** Schematic representation of the subdivision scheme used to map the receptor densities and zinc labeling. The hippocampal formation in the pigeon comprises seven regions: the V-complex, consisting of the ventrolateral (Vl) and ventromedial (Vm) cell bands and the cellular inner triangular region (Tr), the dorsomedial region DM and its ventral (DMv) and dorsal (DMd) subdivisions, and the dorsolateral region DL and its ventral (DLv) and dorsal (DLd) subdivisions. Scale bar = 500 μm.

were labeled with tritiated ligand (total binding). Coincubation of the tritiated ligand and a 1,000–10,000-fold excess of an appropriate nonlabeled ligand (displacer) determined nonspecific and thus nondisplaceable binding. Specific binding is the difference between total and nonspecific binding. 3) A final rinsing step eliminated unbound radioactive ligand from the sections.

The following binding sites were labeled according to the above-cited protocols: 1) α-amino-3-hydroxy-5-methyl-4-isoxalone propionic acid (AMPA) receptor with

TABLE 1.

Incubation Conditions Used for Receptor Autoradiography

Receptor	^{3}H ligand (incubation concentration)	Displacer (incubation concentration)	Incubation buffer	Preincubation step	Main incubation step	Rinsing step
AMPA	[^{3}H]AMPA (10 nM)	Quisqualate (10 μM)	50 mM Tris-acetate (pH 7.2)	3 × 10 min at 4°C in incubation buffer	45 min at 4°C in incubation buffer + 100 mM KSCN	4 × 4 sec at 4°C in incubation buffer + 2 × 2 sec at 4°C in acetone/glutaraldehyde
Kainate	[^{3}H]kainate (8 nM)	Kainate (100 μM)	50 mM Tris-citrate (pH 7.1)	3 × 10 min at 4°C in incubation buffer	45 min at 4°C in incubation buffer + 10 mM Ca-acetate	4 × 4 sec at 4°C in incubation buffer + 2 × 2 sec at 4°C in acetone/glutaraldehyde
NMDA	[^{3}H]MK-801 (5 nM)	MK-801 (100 μM)	50 mM Tris-HCl (pH 7.2)	15 min at 25°C in incubation buffer	60 min at 25°C in incubation buffer + 30 μM glycine + 50 μM spermidine	2 × 5 min at 4°C in incubation buffer
Muscarinergic cholinergic M_1	[^{3}H]pirenzepine (1 nM)	Pirenzepine (10 μM)	Modified Krebs-Ringer buffer (pH 7.4)	20 min at 25°C in incubation buffer	60 min at 25°C in incubation buffer	2 × 5 min at 4°C in incubation buffer
Muscarinergic cholinergic M_2	[^{3}H]oxotremorine-M (0.8 nM)	Carbachol (1 μM)	20 mM Hepes-Tris (pH 7.5) + 10 mM $MgCl_2$	20 min at 25°C in incubation buffer	60 min at 25°C in incubation buffer	2 × 2 min at 4°C in incubation buffer
Nicotinic cholinergic	[^{3}H]cytisine (1 nM)	Nicotine (10 μM)	50 mM Tris-HCl (pH7.4) + 120 mM NaCl + 5 mM KCl + 1 mM $MgCl_2$ + 2.5 mM $CaCl_2$	15 min at 22°C in incubation buffer	90 min at 4°C in incubation buffer	2 × 2 min at 4°C in incubation buffer
α1 Adrenoreceptor	[^{3}H]prazosin (0.2 nM)	Phentolamine (10 μM)	50 mM Tris-HCl (pH 7.4)	30 min at 37°C in incubation buffer	45 min at 30°C in incubation buffer	2 × 5 min at 4°C in incubation buffer
α2 Adrenoreceptor	[^{3}H]UK-14304 (1.4 nM) [^{3}H]RX-821002 (6 nM)	Noradrenaline (100 μM) (-) adrenaline (10 μM)	50 mM Tris-HCl (pH 7.7) + 100 μM $MnCl_2$ 50 mM Tris-HCl (pH 7.4) + 100 mM $MnCl_2$ + 0.1% Ascorbic acid + 0.3 μM 8-OH-DPAT	15 min at 22°C in incubation buffer 30 min at 22°C in incubation buffer	90 min at 22°C in incubation buffer 30 min at 22°C in incubation buffer	5 min at 4°C in incubation buffer 2 × 20 sec at 4°C in incubation buffer
$GABA_A$	[^{3}H]muscimol (6 nM)	GABA (10 μM)	50 mM Tris-citrate (pH 7.0)	3 × 5 min at 4°C in incubation buffer	40 min at 4°C in incubation buffer	3 × 3 sec at 4°C in incubation buffer
Serotoninergic 5-HT_{1A}	[^{3}H] 8-OH-DPAT (1 nM)	Serotonin (10 μM)	170 mM Tris-HCl (pH 7.6) + 4 mM $CaCl_2$ + 0.01% Ascorbic acid	30 min at 22°C in incubation buffer	60 min at 22°C in incubation buffer	1 × 5 min at 4°C in incubation buffer
Dopaminergic $D_{1/5}$	[^{3}H]SCH-23390 (0.5 nM)	SKF 83566 (1 μM)	50 mM Tris-HCl (pH 7.4) + 120 mM NaCl + 5 mM KCl + 2 mM $CaCl_2$ + 1 mM $MgCl_2$ + 1 μM Mianserin	20 min at 22°C in incubation buffer	90 min at 22°C in incubation buffer	2 × 10 min at 4°C in incubation buffer

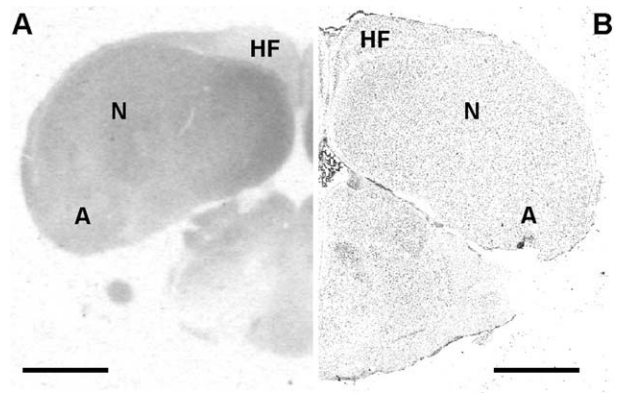

Figure 3. Original autoradiograph and its Nissl-stained counterpart of a coronal forebrain section of the pigeon. **A:** Autoradiograph at atlas level A 5.00 (Karten and Hodos, 1967). Here, binding sites of [^{3}H]muscimol to $GABA_A$ receptors are shown. Darker gray levels indicate higher densities of $GABA_A$ receptors. **B:** Nissl-stained coronal section corresponding to the autoradiograph to trace the borders of the different subdivisions on prints of the digitized autoradiographs. A, arcopallium; HF, hippocampal formation; N, nidopallium. Scale bar = 2 mm.

[^{3}H]AMPA, 2) kainate receptor with [^{3}H]kainate, 3) N-methyl-D-aspartate (NMDA) receptor with [^{3}H]MK-801, 4) γ-aminobutyric acid A ($GABA_A$) receptor with [^{3}H]muscimol, 5) muscarinic cholinergic M_1 receptor with [^{3}H]pirenzepine, 6) muscarinic cholinergic M_2 receptor with [^{3}H]oxotremorine-M, 7) nicotinic cholinergic (nACh) receptor with [^{3}H]cytosine, 8) noradrenergic α_1 adrenoreceptor with [^{3}H]prazosin, 9) noradrenergic α_2 adrenoreceptor with [^{3}H]RX-821002, 10) serotonergic 5-HT_{1A} receptor with [^{3}H]8-OH-DPAT, and 11) dopaminergic $D_{1/5}$ receptors with [^{3}H]SCH 23390. Sections were air dried overnight and subsequently coexposed for 4–5 weeks against a tritium-sensitive film (Hyperfilm; Amersham, Braunschweig, Germany) with plastic ^{3}H standards (Microscales; Amersham) of known concentrations of radioactivity.

Anatomical identification

The borders of the HF subdivisions (Fig. 2) were identified based on previous cytoarchitectural, neurochemical, and tract-tracing studies (Erichsen et al., 1991; Atoji et al., 2002; Kahn et al., 2003; Atoji and Wild, 2004, 2005, 2006; Rosinha et al., 2009). Borders of the different subdivisions were traced on prints of the digitized autoradiographs by projecting the cell body stained sections onto the digitized images of the autoradiographs (Fig. 3).

Image analysis

The resulting autoradiographs were subsequently processed via densitometry with a video-based image analyzing technique (Schleicher et al., 2005). Autoradiographs were digitized by means of a KS-400 image analyzing system (Kontron Germany) connected to a CCD camera (Sony) equipped with an S-Orthoplanar 60-mm macro lens (Zeiss). The images were stored as binary files with a resolution of 512 × 512 pixels and eight-bit

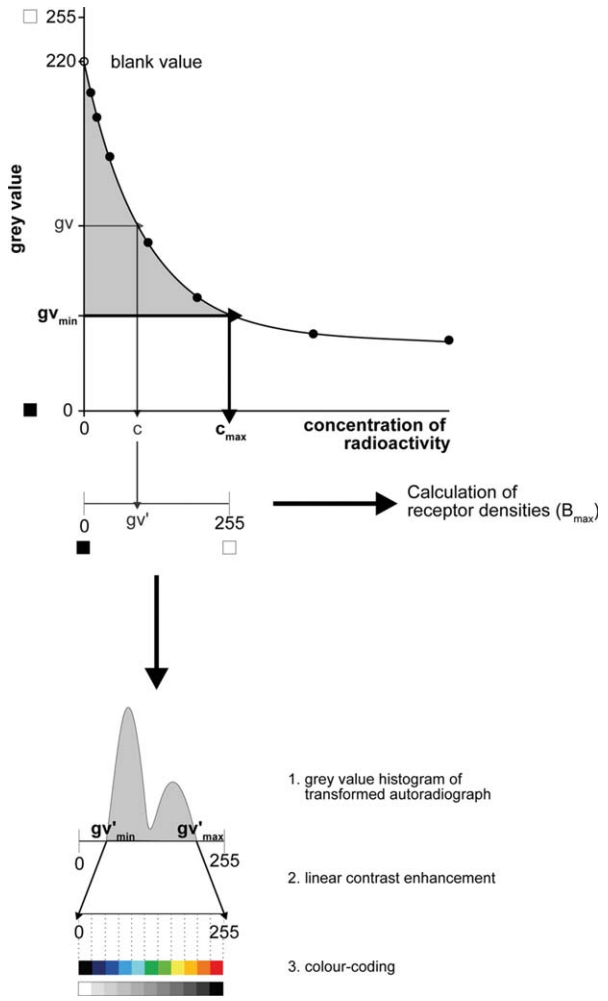

Figure 4. Example of a calibration curve based on isotope standards from which the concentration of bound ligands was calculated. The gray value images of the coexposed microscales were used to compute a calibration curve by nonlinear, least-squares fitting, which defined the relationship between gray values in the autoradiographs and concentrations of radioactivity. This allowed pixel-wise conversion of the gray values of an autoradiograph into the corresponding concentrations of radioactivity. A gray-value histogram of the transformed autoradiograph was built, followed by a linear contrast enhancement procedure. After that, the autoradiograph was color coded as indicated in the graph. The concentrations of binding sites occupied by the ligand under incubation conditions are transformed into fmol/mg protein at saturation conditions by means of the equation $(K_D + L)/A_S \times L$, where K_D is the equilibrium dissociation constant of ligand-binding kinetics, L is the incubation concentration of ligand, and A_S is the specific activity of the ligand.

gray value. The gray-value images of the coexposed microscales were used to compute a calibration curve by nonlinear, least-squares fitting, which defined the relationship between gray values in the autoradiographs and concentrations of radioactivity that were then indicated in the color-coded autoradiographs (see Fig. 4). This allowed the pixel-wise conversion of the gray values of an autoradiograph into the corresponding concentration of radioactivity. The concentrations of binding sites occupied by a ligand under incubation conditions are transformed into fmol/mg protein at saturation conditions by means of the equation $(K_D + L)/A_S \times L$, where K_D is the equilibrium dissociation constant of ligand-binding kinetics, L is the incubation concentration of ligand, and A_S is the specific activity of the ligand.

For the analysis of each ligand for each subdivision for a given pigeon, we attempted to sample HF, in the left hemisphere, at six evenly distributed anterior–posterior levels between A 9.5 and A 4.0 according to the atlas of Karten and Hodos (1967). However, for some ligands in some individuals, the tissue was not of sufficient quality to carry out an analysis at all six levels, and receptor concentrations were derived from the tissue available and based on fewer than six sections. Also, not all subdivisions extend across the entire anterior–posterior range sampled. For example, the V-complex is not discernible at more anterior levels, and DLd and DMd are not discernible at more posterior levels (Fig. 2); as a result, fewer than six sections were used for these subdivisions. The mean of the gray values contained in a specific HF subdivision over the sampled AP levels from one animal was then transformed into a receptor concentration (fmol/mg protein). The mean of each ligand in each subdivision averaged across the six animals was then reported as the receptor concentration. All receptor-binding densities are presented as mean ± SEM. Quantitative, multireceptor data are presented in regional fingerprints that were prepared as polar plots that separately show the density of a single receptor type for all subdivisions (Fig. 5).

Statistical analysis

For comparisons (see below), it was useful to determine whether any difference in receptor densities among the HF subdivisions, either visually or quantitatively revealed, was statistically verifiable. To do this, we first applied a Friedman ANOVA across all subdivisions for each ligand. If significant, pair-wise comparisons were run with the Wilcoxon-rank test. For all statistical analyses, Statistica 10 (StatSoft, Tulsa, OK) was used. The significance level was set at 0.05.

Zinc labeling

For the zinc-labeling procedure, an additional five adult pigeons of unknown sex obtained from local breeders were used. Pigeons were housed in individual cages (30 × 30 × 45 cm) in a temperature (21°C ± 1°C)- and humidity-controlled room with a 12-hour light–dark circle. The subjects had access to grit, food, and water ad libitum. All experimental procedures were approved by national authorities (LANUV NRW, Germany) and were carried out in accordance with the National Institutes of Health *Guide for care and use of laboratory animals*. All subjects were transcardially perfused for 5 min with a 0.1% Na_2S in phosphate-buffered solution (105 mM $NaH_2PO^4 \cdot 2H_2O$ in distilled H_2O, pH set to 6.35 with NaOH) using an average pressure of 15 ml/min (modified from Danscher and Zimmer, 1978). The brain was removed and incubated for 3 hours in a 5% phosphate-buffered Acrolein solution for immersion fixation, followed by rinsing for twice for 30 min and twice for 5 min in PB. After incubation for 24 hours in 30% sucrose in PB for cryoprotection, brains were cut into 25-μm thin frontal sections using a microtome (Leica Microsystems, Wetzlar, Germany). Every tenth section was mounted on slides. Slides were rinsed for 5 min in distilled water and briefly dried at 30°C.

For the zinc staining, four solutions were prepared. 1) Gum arabic, 450 g, was dissolved in 900 ml distilled H_2O and stirred for 5 days. After a few hours of precipitation, the supernatant was collected and the precipitate discarded. The Gum arabic solution can be stored at −20° until further use. 2) Citric acid monohydrate ($C_6H_8O_7 \cdot H_2O$), 5 g, was dissolved in 12.5 ml distilled H_2O. After complete dissolving of citric acid monohydrate, 4.85 g trisodium citrate dihydrate ($Na_3C_6H_5O_7 \cdot 2H_2O$) was added to the solution. The solution was then filled to 20 ml with distilled H_2O. 3) Hydroquinone, 1.7 g, was dissolved in 30 ml distilled H_2O. 4) Silver nitrate, 0.21 g, was dissolved in 30 ml distilled H_2O. Because the solution is light sensitive, it has to be protected from light all the time.

One hundred twenty-five milliliters of the gum arabic solution was mixed with solutions 2–4 and stirred for 5 min. The emergent developer solution was poured into an opaque plastic box, and sections were incubated in the developer solution for 3–4 hours. When staining had reached a sufficient intensity, as determined visually, the sections were removed from the developer solution and washed under running tap water for 15 minutes. After incubation in H_2O overnight, slices were dehydrated and embedded/coverslipped in DPX (Sigma-Aldrich). It was crucial to use high-grade H_2O to

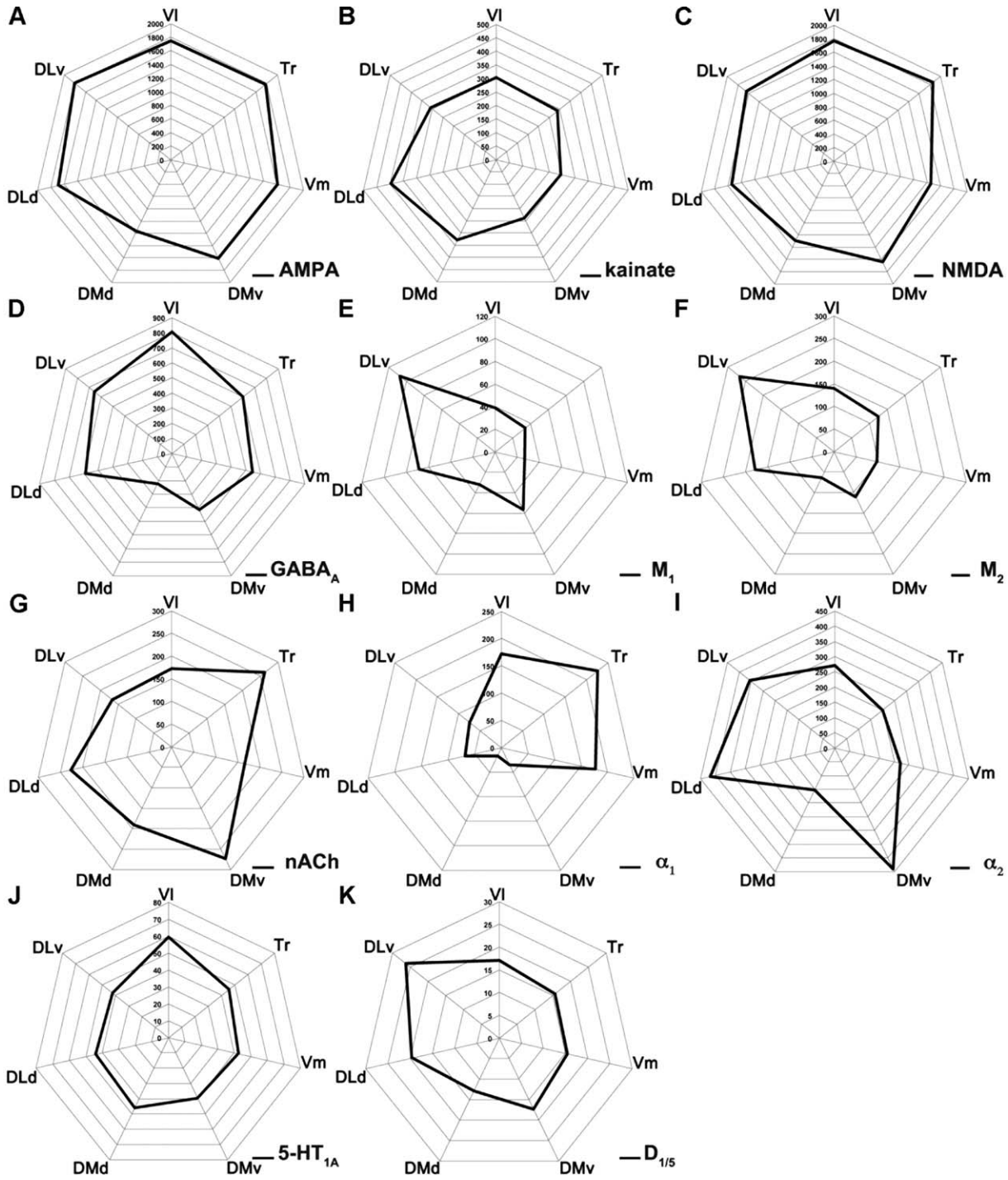

Figure 5. Receptor fingerprints of the pigeon hippocampal formation (HF) subdivisions. The coordinate polar plots (*A–K*) show the individual receptor densities in fmol/mg protein for all subdivisions. The black lines connecting the mean densities of the receptors in each subdivision define the shape of the fingerprint so the reader can quickly notice substantial differences in the distribution of receptors in all subdivisions of the HF. As demonstrated in the fingerprint, glutamatergic AMPA and NMDA receptors are very similarly distributed in the pigeon HF, with high densities in all areas and a decline in DMd, whereas the high kainate receptors densities in DMd and DLd cause a peak in these subdivisions. $GABA_A$ receptor densities peaked in the Vl region and showed a decline in DMd. Muscarinic M_1 and M_2 receptors showed the same fingerprint shape. Densities differed substantially between DLv and the other subdivisions, which resulted in a substantial peak in the west–north direction of their polar plots. By contrast, nicotinic receptors were densely distributed in DMv, Tr, and DLd. Noradrenergic α_1 and α_2 substantially differed in their distributions. Very intense labeling for α_1 was found in the V-complex, so the northeast direction dominates the shape of its fingerprint. By contrast, α_2 receptor levels were high in DMv and the DL regions. 5-HT_{1A} receptor distributions, although with much lower densities, were similar to the $GABA_A$ receptor distributions but showed no break in DMd. Finally, $D_{1/5}$ receptor distribution was similar to the M_2 distribution. Note that the scales in A–K are different. DMd, dorsal part of the dorsomedial region of HF; DMv, ventral part of the dorsomedial region of HF; DLd, dorsal part of dorsolateral region of HF; DLv, ventral part of dorsolateral region of HF; Tr, triangular region of the ventromedial region of HF; Vm, ventromedial part of the V-complex; Vl, ventrolateral part of the V-complex.

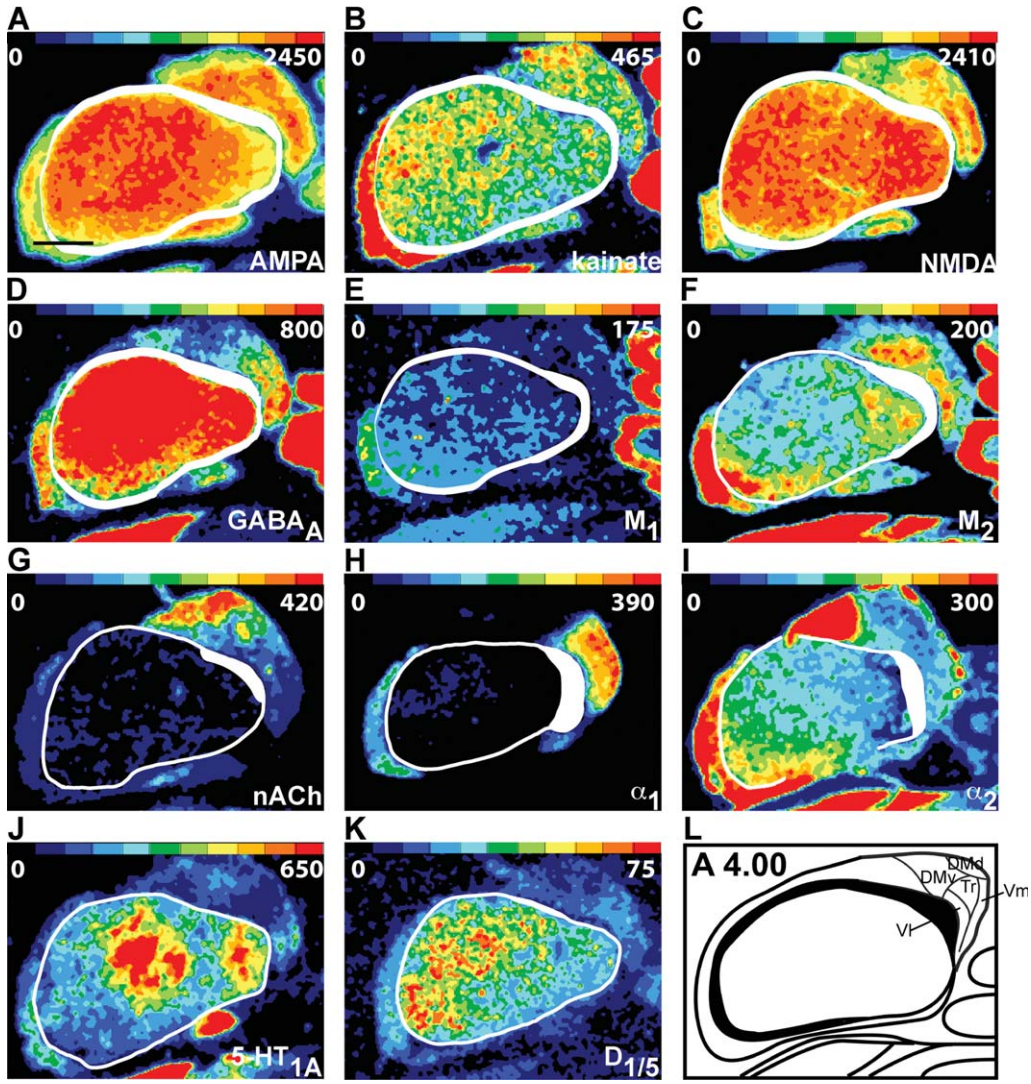

Figure 6. Color-coded autoradiographs showing the distribution and density of AMPA, kainate, NMDA, $GABA_A$, M_1, M_2, nicotinic cholinergic (nACh), α_1, α_2 5-HT_{1A}, and $D_{1/5}$ receptors in coronal sections through the pigeon HF around rostrocaudal level A 4.00 (**A–L**). Densities can be read using the scale for each receptor on the top of each autoradiograph. Note that the end of the red scale indicates the best fit for the investigated HF substructures but not the maximal densities. White outlines show the location of the ventricle. Scale bar = 1.3 mm.

prevent any metal or chloride ions from contaminating working solutions or labware until completing incubation in developer solution, because such ions can interfere with autometallographic zinc labeling.

Sections were analyzed with a Zeiss Axio Imager M1 Microscope (Carl Zeiss) with ×2.5 objective. HF images at A 9.50, A 8.00, A 6.50, and A 5.00 (according to the atlas of Karten and Hodos, 1967) were taken with an AxioCam MRM (Carl Zeiss) and the software AxioVison 4.8 (Carl Zeiss) with an exposure time of 8.4 msec.

To demonstrate that the observed labeling was specific to zinc, we carried out two control procedures. One control pigeon was perfused without using Na_2S. For a second control pigeon, the developer solution was prepared without silver nitrate. Further steps were performed as described above.

RESULTS

Figure 2 displays representative Nissl-stained sections and schematic images of the HF subdivisions used to map the receptor radiographs and zinc labeling. Beginning ventromedially and moving dorsolaterally, we subdivided HF into a ventromedial region (V-complex) with a medial cell layer (Vm), triangular region (Tr), lateral cell layer (Vl), dorso-dorsomedial region (DMd), ventro-dorsomedial region (DMv), dorso-dorsolateral region (DLd) and ventro-dorsolateral region (DLv).

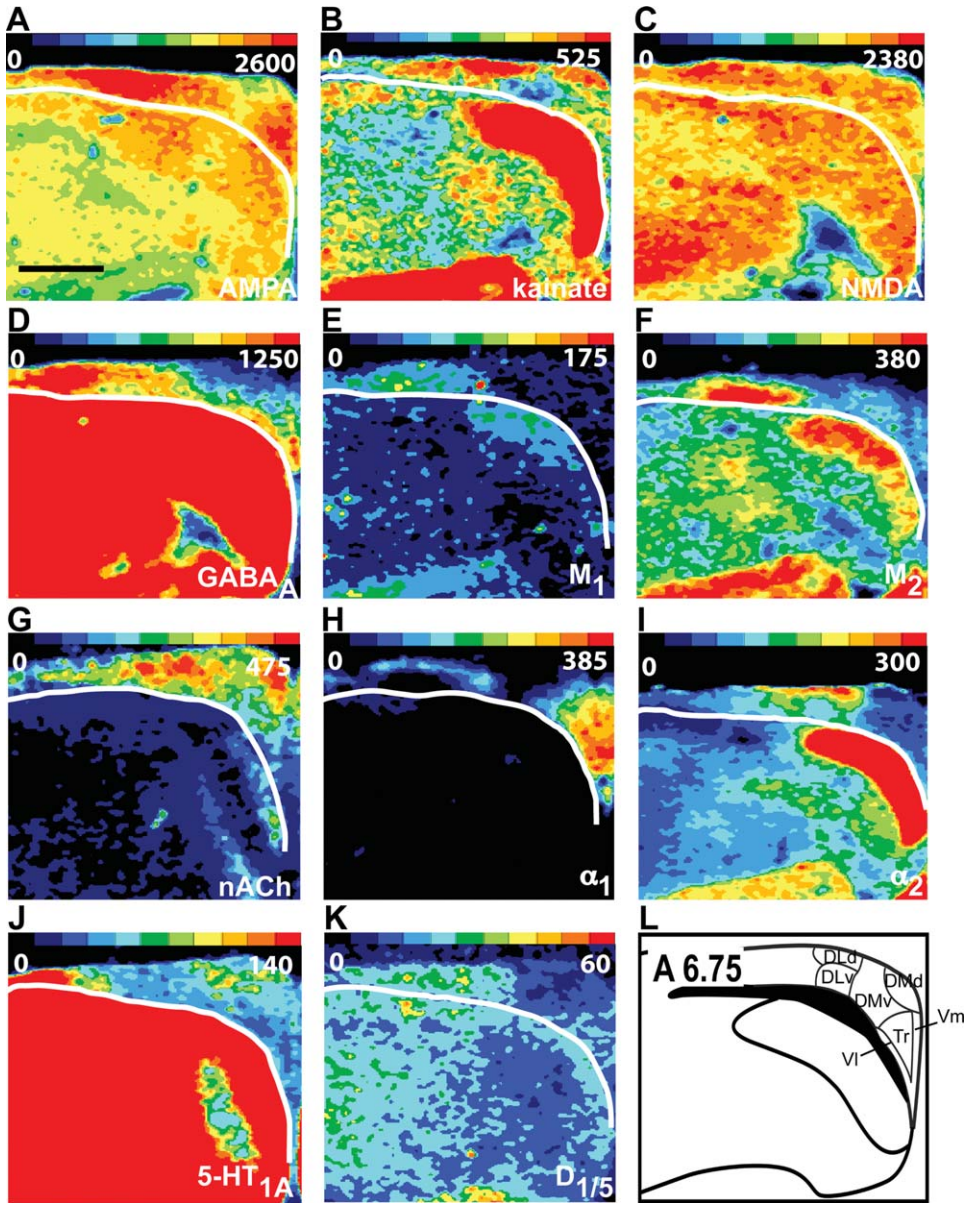

Figure 7. Color-coded autoradiographs showing the distribution and density of AMPA, kainate, NMDA, $GABA_A$, M_1, M_2, nicotinic cholinergic (nACh), α_1, α_2 5-HT_{1A}, and $D_{1/5}$ receptors in coronal sections through the pigeon HF around rostrocaudal level A 6.50 (**A–L**). Densities can be read using the scale for each receptor on the top of each autoradiograph. Note that the end of the red scale indicates the best fit for the investigated HF substructures but not the maximal densities. The white outlines show the location of the ventricle. Scale bar = 1.1 mm.

Receptor-binding site densities in the HF

Binding site densities of all receptors are presented in a two-dimensional polar coordinate plot to construct a multireceptor fingerprint for each analyzed receptor for all HF subdivisions (see Fig. 5). Glutamatergic AMPA and NMDA receptors and GABAergic $GABA_A$ receptors displayed the highest densities. By contrast, muscarinergic cholinergic M_1, serotonergic 5-HT_{1A}, and dopaminergic $D_{1/5}$ receptors displayed low densities throughout HF (see Fig. 5). As illustrated in the color-coded autoradiographs, in general, most of the HF subdivisions were labeled by glutamate and $GABA_A$ receptors, and it is noteworthy that noradrenergic α_1 and α_2 receptors nicely resolved some subdivisions (Figs. 6, 7). All receptor binding site densities are given in fmol/mg protein.

AMPA

Comparisons between all studied subdivisions using a Friedman ANOVA showed significant regional differences

of the AMPA receptor densities (χ^2 [N = 6, df = 6] = 25.64, $P < 0.001$). AMPA receptor concentrations varied from 1,164 ± 77 fmol/mg in DMd to 1,802 ± 58 fmol/mg in Dlv (Figs. 5–7). A high receptor density was also found in Tr (1,777 ± 80 fmol/mg). In general, densities of the dorsolateral subdivisions were higher than those of the dorsomedial subdivisions, with DMd showing the lowest binding site densities among the dorsal regions. Densities in DLd were higher than densities in DMd (N = 6, T = 1, $P < 0.05$), and DLv was different from DMv and DMd (both N = 6, T = 0, $P < 0.05$). AMPA receptor labeling clearly separated DMd and DMv from the V-complex, which showed higher binding site densities. DMv and DMd showed lower densities of AMPA receptors than Tr and Vl (all N = 6, T = 0, $P < 0.05$), and only DMd was additionally different from Vm (N = 6, T = 0, $P < 0.05$). DMd was also different from DMv. DMv displayed a binding site density of 1,611 ± 67 fmol/mg, which was about 50% higher compared with DMd (N = 6, T = 0, $P < 0.05$). Within the V-complex, the higher receptor density in Tr can be distinguished from Vm (N = 6, T = 0, $P < 0.05$).

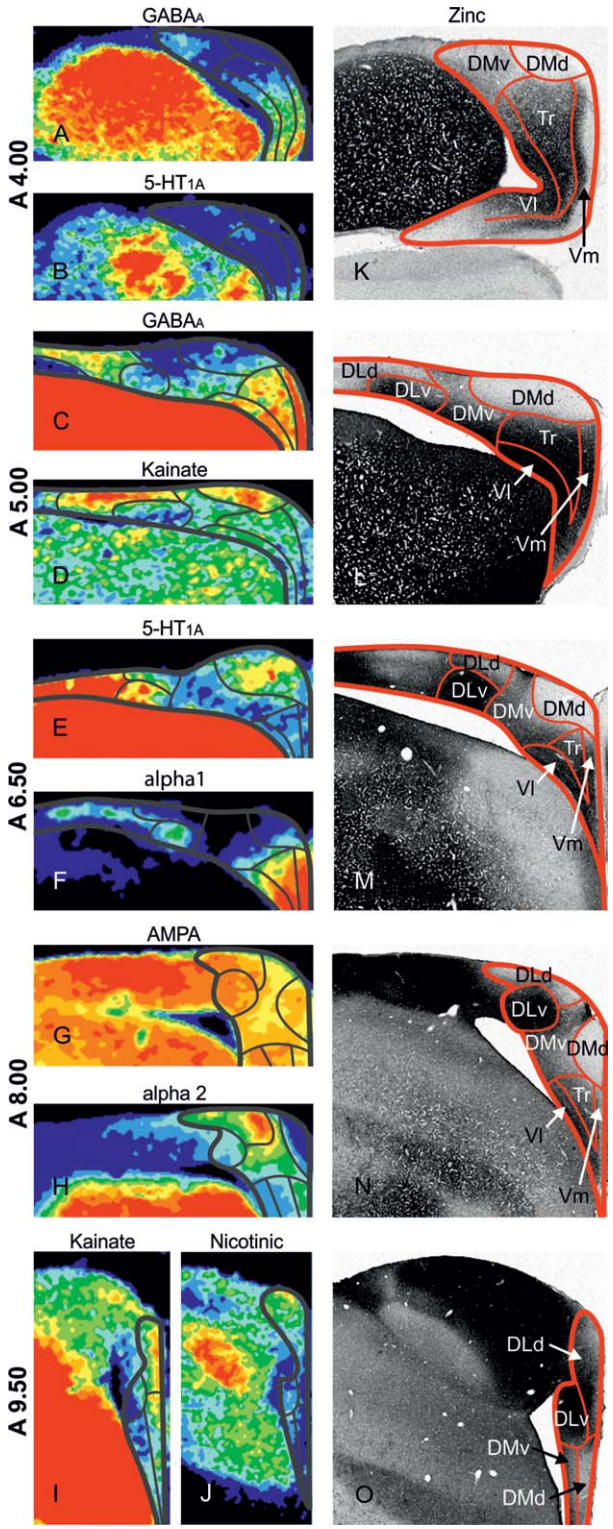

Figure 8. Color-coded autoradiographs and zinc labeling in the pigeon hippocampal formation (HF). **A–J:** Color-coded autoradiographs of selected receptors at selected rostrocaudal levels from A 4.00 to A 9.50 highlighting subdivision differences designated by different receptor densities. Red areas indicated high receptor densities; blue areas showed low receptor densities. **K–O:** Subdivision differences in zinc labeling observed in the pigeon HF from rostrocaudal levels A 4.00 to A 9.50. Black areas were high in zinc, and light gray areas were low in zinc.

Kainate

The densities of kainate receptors varied between the HF subdivisions (χ^2 [N = 6, df = 6] = 29.50, $P < 0.001$). Highest densities for kainate receptors were detected in DLd (398 ± 15 fmol/mg) and lowest in DMv (238 ± 23 fmol/mg; Figs. 5–7). In the dorsolateral region, DLd and DLv showed different binding site densities (N = 6, T = 0, $P < 0.05$). More than any other ligand, labeling of kainate in DMd, with a concentration of 328 ± 23 fmol/mg, clearly separated it from surrounding subdivisions as DMd displayed lower densities than DLd and higher densities than DMv (both N = 6, T = 0, $P < 0.05$; Fig. 8). In the V-complex, a stepwise decrease in kainate binding site concentration could be observed from Vl (303 ± 29 fmol/mg) to Tr (289 ± 27 fmol/mg) to Vm (245 ± 23 fmol/mg; Vl and Tr: N = 6, T = 1, $P < 0.05$; Tr and Vm: N = 6, T = 0, $P < 0.05$; Vl and Vm: N = 6, T = 0, $P < 0.05$; Fig. 5).

NMDA

Similarly to AMPA receptors, NMDA receptors were highly expressed in HF. The Friedman ANOVA revealed a significant overall effect (χ^2 [N = 6, df = 6] = 26.57, $P < 0.001$). The highest amounts of NMDA labeling were detected in Tr (1,855 ± 83 fmol/mg) and the

lowest in DMd (1,297 ± 76 fmol/mg; Figs. 5–7). Binding site densities for NMDA receptors were homogeneously distributed throughout DLd (1,543 ± 141 fmol/mg) and DLv (1,646 ± 85 fmol/mg; N = 6, T = 5, n.s.). Dorsomedially, DMv showed considerably higher concentrations of NMDA receptor labeling (1639 ± 98 fmol/mg) than DMd (N = 6, T = 0, $P < 0.05$). Furthermore, DMv was clearly distinct with respect to the V-complex (DMv and Tr: N = 6, T = 0, $P < 0.05$; DMv and Vl and DMv and Vm: both N = 6, T = 1, $P < 0.05$). In the V-complex, Tr showed a higher density of NMDA receptors compared with Vm (N = 6, T = 0, $P < 0.05$) but not Vl (N = 6, T = 2, n.s.). However, Vl showed a higher density (1,768 ± 82 fmol/mg) than Vm (1,456 ± 93 fmol/mg; N = 6, T = 0, $P < 0.05$). Notably, NMDA displayed a relatively more homogeneous binding site pattern in rostral HF compared with the more regionally distinctive pattern in caudal HF (Figs. 6, 7).

$GABA_A$

$GABA_A$ receptor densities varied from 807 ± 72 fmol/mg protein in Vl to 221 ± 33 fmol/mg in DMd (χ^2 [N = 6, df = 6] = 28.79, $P < 0.001$; Figs. 5–8). The dorsolateral regions DLd (588 ± 54 fmol/mg) and DLv (658 ± 40 fmol/mg) showed an approximately threefold higher receptor concentration compared with DMd (221 ± 33 fmol/mg). DMd showed lower $GABA_A$ receptor density than DLv, DLd, and DMv (all N = 6, T = 0, $P < 0.05$), and DMv (415 ± 55 fmol/mg) showed lower densities than DLd (N = 6, T = 1, $P < 0.05$) and DLv (N = 6, T = 0, $P < 0.05$). Furthermore, DMv and DMd differed from all V-complex subdivisions (all N = 6, T = 0, $P < 0.05$, except for DMv and Vm: N = 6, T = 1, $P < 0.05$). Indeed, the low $GABA_A$ receptor densities in DMd and DMv clearly separate the entire DM from the neighboring ventromedial and dorsolateral regions (Figs. 6–8). In the V-complex, $GABA_A$ receptor densities decreased from Vl (807 ± 72 fmol/mg) to Tr (601 ± 57 fmol/mg) to Vm (546 ± 43 fmol/mg; Figs. 5–8). However, significant differences could be detected only between Vl and Tr (N = 6, T = 0, $P < 0.05$) and Vl and Vm (N = 6, T = 0, $P < 0.05$).

M_1

Muscarinergic cholinergic M_1 receptors were barely detectable throughout HF (Figs. 5–7). Modestly high receptor densities could be seen in DLd (69 ± 7 fmol/mg) and DLv (107 ± 5 fmol/mg). In the rest of HF, M_1 receptor density ranged between 27 ± 3 fmol/mg in Vm and 57 ± 7 fmol/mg in DMv. Statistical analysis revealed a significant regional overall effect (χ^2 [N = 6, df = 6] = 34.64, $P < 0.001$). Subsequent post hoc analyses showed that all subdivisions displayed different densities of M_1 receptors compared with each other (all N = 6, T = 0, $P < 0.05$), except for the comparisons between DLd and DMv (N = 6, T = 4, n.s.) and DMd and Tr (N = 6, T = 5, n.s.; Figs. 5–7).

M_2

M_2 receptor binding resulted in a clear parcellation of HF into its subdivisions (Figs. 5–7). Lowest densities were detected in DMd (64 ± 13 fmol/mg), with highest densities (267 ± 24 fmol/mg) in DLv. The Friedman ANOVA resulted in a significant overall effect (χ^2 [N = 6, df = 6] = 29.43, $P < 0.001$). DLv showed higher amounts of M_2 receptors than DLd (179 ± 13 fmol/mg; N = 6, T = 1, $P < 0.05$) and DMv (111 ± 22 fmol/mg; N = 6, T = 0, $P < 0.05$). The densities of M_2 receptor in DMd were lower than in all other regions (all N = 6, T = 0; $P < 0.05$). Receptor density decreased from Vl (140 ± 20 fmol/mg) to Tr (125 ± 23 fmol/mg; N = 6, T = 0, $P < 0.05$) to Vm (97 ± 14 fmol/mg protein; compared with Tr N = 6, T = 1, $P < 0.05$). DMv densities were not different from any subdivision of the V-complex (Vl N = 6, T = 3, n.s.; TR and Vm N = 6, T = 6, n.s.; Figs. 5–7).

nACh

Binding sites for nACh receptors showed an inverse pattern of densities in DLd and DLv compared with both muscarinergic cholinergic receptor types (Figs. 5–8). A significant overall effect was detected with the Friedman ANOVA (χ^2 [N = 6, df = 6] = 27.57, $P < 0.001$). The concentration of nACh receptors was higher in DLd (228 ± 22 fmol/mg) compared with DLv (167 ± 16 fmol/mg; N = 6, T = 0, $P < 0.05$). Highest binding site density was detected in DMv (273 ± 31 fmol/mg). DMd (190 ± 18 fmol/mg) displayed a lower binding density for nACh receptors than DMv and DLd (both N = 6, T = 0, $P < 0.05$). Density for nACh receptors in DMv was also higher compared with DLd, DLv, Vl (172 ± 15 fmol/mg) and Vm (166 ± 18 fmol/mg; all N = 6, T = 0, $P < 0.05$) but not Tr (262 ± 32 fmol/mg; Figs. 5–8).

α_1

The Friedman ANOVA revealed a significant regional effect of noradrenergic α_1 receptors in the pigeon HF (χ^2 [N = 6, df = 6] = 31,57, $P < 0.001$). Noradrenergic α_1 receptors were detected at only 16 ± 1 fmol/mg in DMd, but substantially higher amounts of 226 ± 11 fmol/mg were found in Tr (Figs. 5–8). DLd (67 ± 5 fmol/mg) and DLv (74 ± 4 fmol/mg) displayed intermediate densities of α_1 adrenoreceptors. Vl (172 ± 14 fmol/mg) and Vm (177 ± 27 fmol/mg) showed similar α_1 receptor densities. The α_1 receptor binding with [^{3}H]prazosin generally rendered the entire V-complex

distinctive (Figs. 6–8). DMv displayed at least a fourfold lower density (36 ± 4 fmol/mg) than any ventromedial region and was distinct from all other regions (all N = 6, T = 0, $P < 0.05$). The lowest density of noradrenergic α_1 receptors in the HF was detected in DMd (all N = 6, T = 0, $P < 0.05$).

α_2

Whereas α_1 adrenoreceptors were highly expressed in the V-complex, α_2 adrenoreceptors showed high densities in the dorsolateral and dorsomedial regions. Densities of α_2 adrenoreceptors in the HF varied from 441 ± 48 fmol/mg in DMv to 153 ± 19 fmol/mg in DMd (Figs. 5–8). The Friedman ANOVA detected a significant regional overall effect (χ^2 [N = 6, df = 6] = 30.07, $P < 0.001$). Densities of α_2 adrenoreceptors in DMd were threefold lower than in DMv (N = 6, T = 0, $P < 0.05$; Figs. 5–7). Densities in DMv were also higher in comparison with the regions of the V-complex (Vl & Tr N = 6, T = 0, $P < 0.05$; Vm N = 6, T = 1, $P < 0.05$). In the V-complex, Vl (271 ± 28 fmol/mg) showed higher densities than Tr (201 ± 21 fmol/mg; N = 6, T = 0, $P < 0.05$) but not Vm (220 ± 19 fmol/mg; N = 6, T = 4, $P = 0.17$). The noradrenergic α_2 adrenoreceptors were also abundant but unequally distributed in DLd (418 ± 31 fmol/mg) and DLv (354 ± 18 fmol/mg; N = 6, T = 0, $P < 0.05$).

5-HT_{1A}

The expression of serotonergic 5-HT_{1A} receptors was generally low throughout the pigeon HF (Figs. 5–8), and no significant regional overall differences were detected (χ^2 [N = 6, df = 6] = 10.00, $P = 0.15$). However, a notably stronger signal could be found in DMd in some sections, especially at the border between DMd and DMv (see, e.g., Fig. 8). However, this stronger signal seemed to be highly variable across pigeons; no significant difference was detected between DMd (46 ± 3 fmol/mg) and neighboring DMv (40 ± 3 fmol/mg), DLd (44 ± 5 fmol/mg), or DLv (42 ± 3 fmol/mg). Densities in the V-complex varied and showed the highest value in Vl (60 ± 10 fmol/mg).

$D_{1/5}$

Dopaminergic $D_{1/5}$ receptors showed the lowest densities of all measured receptor types (Figs. 5–7). However, the Friedman ANOVA detected a significant regional overall effect (χ^2 [N = 6, df = 6] = 22.86, $P < 0.001$). The maximal density was 26 ± 3 fmol/mg in DLv (all comparisons N = 6, T = 0, $P < 0.05$; except for the comparison between DLv & DLd N = 6, T = 1, $P < 0.05$). Although $D_{1/5}$ receptors provided little obvious separation among the HF subdivisions, the boundary between DMd and DMv was rendered distinctive by an almost complete lack of $D_{1/5}$ receptors in DMd (Figs. 5–7). DMd showed the lowest receptor density compared with all other DM and DL structures (13 ± 1 fmol/mg; all N = 6, T = 0, $P < 0.05$).

Zinc staining

Although we did not see distinct layers of mossy fibers as found in rat hippocampus (but see Discussion), there is heterogeneity in the density of labeling that maps remarkably well onto our subdivision boundaries (Fig. 8). Moving from ventromedially to dorsolaterally, high zinc density indicated by the dense black labeling is clearly seen throughout Vl, Vm, and Tr. This dense labeling is diminished in DMv, and labeling is virtually nonexistent in DMd. In dorsolateral DLv, dense labeling is seen again, but moderate labeling, similarly to DMv, is seen in DLv. The zinc data clearly indicate a well-defined boundary between the rich labeling in the V-complex and the absence of labeling in DMd. Also noteworthy is that zinc does not seem to distinguish between DMv and DLv.

DISCUSSION

Summary of main findings

By using receptor autoradiography for 11 different neurotransmitter receptors and zinc staining, we show that the hippocampal formation of the pigeon can be subdivided into seven subdivisions, which match well with other subdivisional schemes based on neurotransmitter distribution (Erichsen et al., 1991) and connectivity (Kahn et al., 2003; Atoji and Wild, 2004). Additionally, our data offer a further basis for comparing subdivisions of the mammalian and avian hippocampal formation. Our approach has the advantage that we can compare the receptor architecture of an evolutionarily ancient brain structure, which retains a similar role in spatial cognition in species that have had independent evolutionary histories for about 300 million years. Similarities between birds and mammals may offer insight into how selective pressure may conserve basic receptor traits regardless of structural differences. In addition, it remains uncertain whether clear similarities exist among the subdivisions of avian and mammalian HF. Therefore, an important goal of our study was to compare the receptor architecture of the pigeon and mammalian HF to assess better which, if any, avian subdivisions may correspond best to the mammalian hippocampal DG, CA fields, subiculum, and EC.

Subdivisional organization of the avian hippocampal formation: previous studies

Different criteria have been used to define subdivisions of the HF in diverse bird species (Casini et al.,

1986; Erichsen et al., 1991; Krebs et al., 1991; Montagnese et al., 1996; Székély, 1999; Atoji et al., 2002; Kahn et al., 2003; Atoji and Wild, 2006; Nair-Roberts et al., 2006; Suarez et al., 2006; Mayer et al., 2009; Sherry, 2011). During the first part of the twentieth century, judging from comparative studies between reptiles and different types of mammals (e.g., rodents, insectivores, and chiroptera; Rose, 1912) and birds (e.g., chicken and pigeons; Rose, 1914), Rose divided the caudal part of the avian dorsomedial forebrain into a ventrally located Ammon's formation and a dorsally located entorhinal area, which, in his opinion, were comparable to the similarly named regions in mammals (Rose, 1914, 1926). In 1930, Craigie studied the kiwi's (*Apteryx australis*) brain and named the dense cellular layer between Rose's Ammon's formation and entorhinal area the *fascia dentate*, which was not included in Rose's earlier analysis. A few years later, Craigie (1935) studied the emu's (*Dromiceius novaehollandiae*) brain. He introduced the terms *hippocampal area* and *parahippocampal area* (APH) based on cell types and their arrangement. However, a clear border between the ventral and dorsal parts of HF as well as between the APH and the hyperpallium apicale (HA) were not defined. Furthermore, the HF in most other bird species is considerably smaller than that in the emu, so the emu classification is difficult to apply to other bird species.

Using Nissl staining and the previous data, Karten and Hodos (1967) divided the pigeon hippocampal formation into two regions, a hippocampus proper and the APH. Analysis of neurotransmitters and related enzymes with immunohistochemical methods offered the first higher resolution HF subdivision scheme and revealed seven candidate subdivisions (Erichsen et al., 1991; Krebs et al., 1991). A later electrophysiological study was able to resolve five of these subdivisions (Siegel et al., 2000). Probably the most influential subdivisional scheme of the avian HF comes from the work of Atoji and Wild (2004, 2006). Using tract tracing and Nissl staining, they divided the pigeon hippocampal formation into a dorsomedial region (DM), a dorsolateral region (DL), a medial V-complex region (V), which included a triangular region (Tr) with adjacent ventromedial (Vml) and ventrolateral (Vll) cell layers. Also located dorsomedially were three smaller areas, a magnocellular (Ma), a parvocellular (Pa), and a cell-poor (Po) region (Atoji and Wild, 2004, 2006). Additionally, Atoji and Wild (2004, 2006) showed that DM could be further subdivided into a lateral portion (DMl) and a medial portion (DMm). DL could also be further subdivided into a dorsal portion (DLd) and a ventral portion (DLv). It is the subdivisional scheme of Atoji and Wild (2004) that we used to create our provisional subdivisional map, and indeed it is remarkable how well many of the receptors studied here, as well as the zinc labeling, respected the borders of these subdivisions.

Boundaries and subdivisions of the pigeon HF based on receptor autoradiography

Consistent with earlier studies using immunohistochemical (Krebs et al., 1991; Erichsen et al., 1991) and tract tracing (Atoji and Wild, 2004, 2006; Kahn et al., 2003) analyses, the receptor data indicated relatively sharp boundaries between the most lateral portions of HF, namely, DLd and DLv, and laterally adjacent areas (for some examples see Figs. 6–8). The border between HA and dorsolateral HF was especially visible with AMPA, $GABA_A$, M_2, α_1, α_2, and 5-HT_{1A} receptor labeling. Densities of AMPA, $GABA_A$, M_2, and 5-HT_{1A} receptors were higher in HA than in neighboring DLd and DLv, whereas densities of α_1 and α_2 receptors were lower (quantitative HA data not presented).

More posteriorly, dorsolateral HF has been typically distinguished from the neighboring dorsolateral corticoid area (CDL) based on its shape; CDL is characterized as a uniformly thin wall, whereas DL decreases in thickness as it approaches CDL laterally (Montagnese et al., 1993; Atoji and Wild, 2004, 2006). Our ligand maps, by contrast, reveal a much clearer boundary. The border between HF and CDL is particularly distinct with $GABA_A$, M_2, α_1, α_2, and 5-HT_{1A} receptor labeling (Figs. 6, 7). Densities of $GABA_A$, α_1, and 5-HT_{1A} receptors are higher in the CDL than in dorsolateral HF, whereas M_2 and α_2 receptor densities are lower (quantitative data for CDL not presented; Herold et al., 2011, 2012). Also notable is that in more caudal HF CDL borders DMd and DMv as DLd and DLv disappear (for examples see Fig. 8).

Receptor imaging also allowed identification of a boundary between the HF dorsolateral subdivisions, DLd and DLv, and the adjacent dorsomedial structures, DMd and DMv. Densities of AMPA, kainate, $GABA_A$, M_1, M_2, and α_1 receptors were higher in DLd and DLv, whereas nACh receptors were lower in DLd and DLv compared with, in particular, DMv (Figs. 5–7). In general, the multireceptor mapping supports the identification of seven subdivisions as proposed by Erichsen et al. (1991) and Atoji and Wild (2004, 2006).

Glutamate receptors

Glutamate AMPA and NMDA receptor densities were high in all regions of the pigeon HF. AMPA binding did not vary between DLd and DLv, but clearly separated DL from DMv. Furthermore, DMd displayed a relatively low concentration compared with the other regions and could be clearly separated from DMv. In general, DM

showed lower densities than the surrounding DL and V-complex ventromedial regions. In the V-complex, AMPA binding was lower in Vm compared with Tr. Our results showed higher AMPA densities in the pigeon HF compared with those reported for [^{3}H]AMPA binding in marsh tits (*Parus palustris*) and blue tits (*Parus caeruleus*; Stewart et al., 1999). Furthermore, there seemed to be no differences in AMPA receptor densities between DL (their APH) and DM/V-complex (their Hp) in tits.

An immunhistochemical analysis of glutamatergic AMPA receptor subunits revealed that GluR1, GluR2/3, and GluR4 are expressed in the pigeon HF (Rosinha et al., 2009). Especially GluR1 and GluR2/3 were expressed pre dominantly in so-called IR and T neurons, whereas GluR4 was expressed predominantly in so-called R neurons. IR neurons are multipolar projection neurons, T neurons are triangular pyramidal neurons, and R neurons are ovoid or stellate cells that may be glial cells or local interneurons (Tömböl et al., 2000a; Atoji et al., 2002). Rosinha et al. (2009) observed intense labeling for GluR1 and GluR2/3 in the V-complex, in which we detected high AMPA receptor densities as well.

Generally fewer kainate receptors were expressed compared with NMDA or AMPA, but kainate receptors showed a differential regional distribution pattern. Kainate receptor density reached a maximum in DLd and DMd, and the lowest densities were measured in DMv. Again, DMv was distinct from the surrounding DL, ventromedial regions, and DMd. In the V-complex, a stepwise decrease in receptor density could be detected from Vl to Tr to Vm. We are aware of no other studies that have looked at kainate receptor binding in birds.

NMDA receptor binding discriminated mainly among DMd, DMv, and the V-complex. Highest NMDA receptor densities were found in Vl and Tr, and the lowest densities were detected in DMd. Similarly to AMPA receptors, NMDA receptor binding in the V-complex separated Tr from Vm but not Vl. Furthermore, the pattern of NMDA receptors seemed to become increasingly distinctive in the subdivisions of the more caudal part of HF. Compared with our present results, densitometric measurements of NMDA receptor binding with [^{3}H]MK801 in blue and marsh tits showed the same overall densities in the HF of blue tits and slightly lower densities for marsh tits (Stewart et al., 1999). However, in both marsh and blue tits, there seemed to be only small overall differences in NMDA receptor densities between DL (their APH) and DM/V-complex (their Hp).

$GABA_A$ receptor

Examination of $GABA_A$ receptor densities showed again a clear boundary between HF dorsolateral and dorsomedial regions. Densities decreased overall from DL to DMv to DMd. In addition, DMv was different from the V-complex, which showed higher $GABA_A$ receptor densities. Within the V-complex, a decrease from Vl to Tr to Vm was observed. Earlier binding studies in pigeons did not show differences in $GABA_A$ receptor labeling in the Hp/APH region (Veenman et al., 1994). However, our pattern of $GABA_A$ receptor density is in general agreement with results from other bird species looking at GABAergic neurochemistry. In members of the Corvidae and Paridae, calbindin distribution divides HF into five main regions, and the medial and the lateral branches of what would be the V-complex are different (Montagnese et al., 1993). Glutamate decarboxylase (GAD; an enzyme in GABAergic interneurons) was found homogeneously distributed in the neuropil of the pigeon DM and DL, and in small to medium-sized immunoreactive cells throughout the entire HF (Krebs et al., 1991). The pattern of GAD was approximately coextensive with the calbindin staining of Montagnese et al. (1993). As with the intensely GAD- and calbindin-labeled areas, we found high densities of $GABA_A$ receptors throughout the entire pigeon DL and Vl. By contrast, $GABA_A$ receptors were relatively weakly expressed in DM, particularly in DMd.

Cholinergic receptors

The different cholinergic receptors were each distinctly distributed throughout the HF. M_1 densities were highest, followed by M_2 and nACh. M_1 receptors showed the highest concentration in DLv and lower densities in DLd, DMv, and Tr. A low M_1 receptor density rendered DMd distinct from the other regions. In the V-complex, densities decreased from Vl to Tr to Vm, again showing a difference in receptor profile between the medial and the lateral dense cell layers. A similar receptor distribution pattern was also found for M_2 receptors. By contrast, nACh receptor binding showed higher densities in DLd compared with DLv. Both DLv and DLd were different from DMv, whereas DMv again was not distinguishable from Tr. However, higher densities in Tr separated this region from Vl and Vm.

Analysis of muscarinic (M-type) receptors with [^{3}H]N-methyl scopolamine showed no differences in densities between DM/V-complex (their Hp) and DL (their APH) in quail (*Coturnix coturnix japonica*) but higher amounts of M-type receptors in DL compared with DM/V-complex in starlings (*Sturnus vulgaris*; Ball et al., 1990). The densities of M-type receptors in the quail and starling HF were higher across all major subdivisions compared with our findings in pigeon. Although the difference could be explained by species variation, probably more important is the use of subtype-specific ligands for the

group of M-type receptors in our study. Our binding protocols label M_1 and M_2 subtypes separately, which can explain the higher densities for all M-type receptors found by Ball et al. (1990). Our findings are also in line with an earlier autoradiographic study, which showed only low to moderate densities of M-type receptors, 25–250 fmol/mg protein, in DL and DM/V-complex of the pigeon (Dietl et al., 1988). As with starlings (Ball et al., 1990), pigeons showed higher densities of M-type receptors in DL than in all other HF subregions. Weak labeling of muscarinic cholinergic receptors was found in DMd, but nACh receptors occurred at a relatively high density in DMd (see Fig. 5).

Monoaminergic receptors

Monoaminergic receptors showed highly variable densities in the pigeon HF. Highest densities were observed for noradrenergic α receptors and lowest for $D_{1/5}$ receptors α_1 Receptors were expressed in the V-complex region, with highest densities both in Tr and in Vm. This finding is in contrast to the lower density in Vl. The α_1 receptor density of the V-complex was clearly different from that of DMv. DMv can be separated from DMd, DLd, and DLv by differences in α_1 receptor density. However, DLd and DLv could not be discriminated by their α_1 receptor binding. α_2 Receptor binding was higher in DMv and the DL regions. By contrast, α_2 receptors were more dense in DLd compared with DLv but did not differ from DMv. Again, DMd was rendered distinct by its lower α_2 receptor density compared with DMv, DLd, and DLv. In the V-complex, a relatively homogeneous distribution of α_2 receptors was detected. Vl showed higher densities compared with Tr but not Vm. Our results seem to be in line with the distribution of α_2 receptors in the European starling (Heimovics et al., 2011). Although not quantified in their publication, the autoradiographs of the starling HF look similar to the autoradiographs that we obtained for pigeons.

Serotonergic 5-HT_{1A} receptors did not differ among any of the subdivisions. This has already been reported for DL and the DM/V-complex (APH and Hp, respectively, in Herold et al., 2012). The quantitative result is somewhat surprising, because a higher density in DMd was detected by visual inspection in a number of brain sections (see Figs. 6, 7). Similarly to the neurotransmitter 5-HT labeling in DMd and DMv (DMs and parts of DMi in Krebs et al., 1991), 5-HT_{1A} receptor labeling in our study seemed to slowly decrease from rostral to caudal HF, perhaps obscuring subdivision differences in 5-HT_{1A} receptor density.

Dopaminergic $D_{1/5}$ receptors were differentially distributed between DLv and all other subregions. They reach their highest densities in DLv compared with the other subregions. Additionally, lower $D_{1/5}$ densities were observed in DMd compared with the surrounding regions. As in our results, tyrosine hydroxylase (TH) was detected mainly in the dorsal parts of the pigeon HF (Krebs et al., 1991). In general, the low densities of $D_{1/5}$ receptors observed in the pigeon HF are in line with former studies in pigeons, quails, and chicken (*Gallus gallus*; Dietl and Palacios, 1988; Ball et al., 1995; Schnabel and Braun, 1996; Kleitz et al., 2009).

Comparison with the mammalian hippocampal formation

The avian HF and mammalian hippocampus develop from the same portion of the telencephalon (Kallen, 1962; Rodriguez et al., 2002), share the same cell types (Molla et al., 1986; Tömböl et al., 2000a), and have similar neurochemical profiles (Erichsen et al., 1991; Krebs et al., 1991). A special characteristic of both the avian HF and the mammalian hippocampus is adult neurogenesis (Altman, 1962; Barnea and Nottebohm, 1994; Eriksson et al., 1998; Hoshooley et al., 2005; Ming and Song, 2005; Pytte et al., 2007). The similarities may explain the presumably conserved role of both the avian HF and the mammalian hippocampus in cognition (Sherry et al., 1992; Colombo and Broadbent, 2000). However, the connections to other brain areas, e.g., septum, hypothalamus, brainstem nuclei, and telencephalic sensory processing areas, are not fully identical (Casini et al., 1986; Atoji and Wild, 2006). Furthermore, the cytoarchitectural differences between the avian and the mammalian HF have made it difficult to identify similarities in subdivisional organization (but see Erichsen et al., 1991; Kahn et al., 2003; Atoji and Wild, 2006; Papp et al., 2007).

The mammalian hippocampus is divided into distinct subregions based on anatomical criteria, DG with the hilus region, Ammon's horn (comprising the fields CA1–CA4), and the subiculum (Amaral and Witter, 1989; Insausti, 1993; Amunts et al., 2005; Witter, 2007). Because of the distinct cytoarchitecture of DG and Ammon's horn regions, they can be distinguished from the laterally positioned subiculum and EC. Typically, the CA regions are densely packed with pyramidal neurons, whereas the DG is densely packed with granular cells. In contrast, the avian HF is a more nuclear-like structure, densely packed with heterogeneous populations of neurons with a slow transition into the parahippocampal area (DL). In the mammalian hippocampus, the EC is part of the parahippocampal area (gyrus parahippocampalis) and differs considerably from the hippocampal

regions (Amaral and Witter, 1989; Insausti, 1993; Amunts et al., 2005; Witter, 2007).

Different regions of the avian HF, based on tracing studies, have been proposed to be homologues of the mammalian DG. Székély and Krebs (1996) and Kahn et al. (2003) proposed that DM is a homologue of DG and that the V-complex is a homologue of unspecified CA fields. Atoji and Wild (2004, 2006), by contrast, claimed that DM shows properties of both CA and subiculum, whereas the V-shaped structure (our V-complex), because of its intrinsic connections, seems to be more similar to DG. However, seemingly all researchers agree that DL is comparable to EC (Székély, 1999; Siegel et al., 2002; Atoji and Wild, 2004; Puelles et al., 2007; Rattenborg and Martinez-Gonzalez, 2011).

In general, the receptor autoradiographic analysis of 10 different receptor types in the hippocampus of 11 different mammalian species showed that α_1, M_1, 5-HT_2, $GABA_A$, AMPA, kainate, and NMDA receptor densities were minimally variable across species, whereas α_2, 5-HT_{1A}, and M_2 were highly variably expressed (Palomero-Gallagher, 1999). In many of the species studied and compared with all other hippocampal structures, CA3 showed the lowest receptor densities (Kraemer et al., 1995; Palomero-Gallagher, 1999; Zilles et al., 2000; Cremer et al., 2009). To compare and identify better the subdivision similarities (and differences) between pigeon HF and mammalian hippocampus, we created a summary of the already published receptor data in the mammalian HF (Table 2). This table provides the relative receptor densities for each mammalian hippocampal substructure normalized to the mean value of the investigated receptor type in the total hippocampus. For better comparisons, we also added the relative densities for each substructure of the pigeon HF. As in the pigeon, glutamate receptors showed high densities in the mammalian hippocampus, with higher densities for AMPA and NMDA compared with kainate receptors (Palomero-Gallagher, 1999; Zilles et al., 2000; Topic et al., 2007). In rats (*Rattus norvegicus*) and mice (*Mus musculus*), CA1 showed the highest densities for AMPA and NMDA receptors, followed by DG. In contrast, CA3 and DG were high in kainate receptors (Table 2). Overall, the following conclusions can be drawn: in comparing the relative densities of glutamatergic receptors in the different subdivisions of the rodent hippocampus and pigeon HF, the most striking similarities exist between high kainate receptor densities in Vl, Tr, DMd, and DG/CA3, as well as DLd vs. EC, and low kainate receptor concentrations in Vm/DMv and CA1/CA2. NMDA and AMPA receptor densities were mostly comparable between Vl/Tr/DMv and DG/CA1 (Table 2). Binding of $GABA_A$ receptors with [^{3}H]muscimol showed high receptor densities in the pigeon HF and mammalian hippocampus (Kraemer et al., 1995; Topic et al., 2007; Cremer et al., 2009, 2010). $GABA_A$ receptor densities decreased from Ent to DG to CA1 to CA2 to CA3 in mouse, rat, and marmoset (*Callithrix jacchus*) brains. Again, Vl/Tr/Vm and the DL regions resembled DG/CA1 and EC, respectively. DMv was similar to CA2, and DMd, with its very low $GABA_A$ densities, was comparable to CA3. M receptors were more highly expressed in the marmoset and the rodent hippocampus compared with the pigeon HF, but nACh showed higher densities in pigeons compared with rodents (Pauly et al., 1989; Kraemer et al., 1995; Topic et al., 2007; Wolff et al., 2008; Cremer et al., 2009). In pigeons, cholinergic binding sites nicely discriminated among the different subdivisions; however, no pattern was observed to indicate any correspondence among mammalian and avian hippocampal substructures based on density variation in cholinergic receptors (Table 2). This lack of correspondence may reflect interspecies variability with respect to cholinergic receptor types that may obscure detection of general differences in the hippocampal–cholinergic systems in mammals and birds. The analysis of the monoaminergic receptors revealed that α_2 receptor binding suggests a similarity for CA1/DG and Vl/DMv, whereas lower densities in CA2/CA3 appear to resemble more Tr/Vm/DMd (Table 2; Zilles et al., 1993). 5-HT_{1A} receptors showed comparable relative densities only between DG and Vl and between CA1 and Vm for the rat, but not for mice or other mammals (Table 2; Palomero-Gallagher, 1999). $D_{1/5}$ receptors also suggest a DG more similar to Vl and DMv. The high densities of $D_{1/5}$ receptors in the DL regions are also detected in EC.

Overall, we propose close similarity between DG/CA1 and the Vl/Tr/DMv regions, whereass DMd/Vm might be more comparable to the CA2/CA3 regions. DMd shared several receptor characteristics with CA3, and generally DMv was more similar to CA1 and Vm resembled CA2. The DL regions seemed to be comparable to EC (Fig. 9). This latter finding is in line with the generally accepted similarity between DL and EC (for review see Atoji and Wild, 2006).

Zinc staining

High levels of zinc in the mossy fiber system of rats have led avian researchers to seek a DG equivalent in birds, relying on Timm staining. In previous studies (Faber et al., 1989; Montagnese et al., 1993; Tömböl et al., 2000b) of chick and zebra finch brains, an obvious parallel to DG could not be revealed. An examination of our zinc staining (Fig. 8) also failed to reveal the distinctive labeling suggestive of the layered

TABLE 2.

Comparison of Neurotransmitter Receptor Densities in the Pigeon and Mammalian Hippocampal Formation (HF)[1]

	Relative binding densities in the pigeon HF (%)							Relative binding densities in the mammalian HF (%)					
Receptor	Vl	Tr	Vm	DMv	DMd	DLd	DLv	CA1	CA2	CA3	DG	EC	Species
AMPA	107	109	99	99	71	104	111	109 (1), 114 (2), 117 (5), 102 (6), 110 (4), 115 (7)	90 (1), 87 (2), 94 (5)	86 (1), 78 (2), 94 (5), 95 (4), 90 (7)	97 (1), 104 (2), 95 (5), 98 (6), 96 (4), 94 (7)	68 (6)	Rat, Mouse
Kainate	101	96	81	79	109	132	102	52 (1), 67 (2,6), 59 (5), 71 (4), 63 (7)	74 (1), 58 (2), 69 (5)	140 (1), 127 (2), 174 (5), 116 (4), 113 (7)	124 (1), 113 (2), 132 (6), 97 (5), 113 (4), 125 (7)	134 (6)	Rat, Mouse
NMDA	110	116	91	102	81	96	103	120 (1), 124 (2), 130 (5), 105 (6), 126 (4), 135 (7), 110 (3)	84 (1), 83 (2), 99 (5), 88 (3)	74 (1), 71 (2), 83 (5), 81 (4), 69 (7), 82 (3)	90 (1), 101 (2), 89 (5), 95 (6), 93 (4), 97 (7), 94 (3)	77 (6)	Rat, Mouse, Marmoset
$GABA_A$	147	110	100	76	40	107	120	80 (2), 87 (6), 122 (4), 106 (7), 111 (3)	70 (2), 72 (3)	47 (2), 62 (4), 58 (7), 60 (3)	119 (2), 111 (6), 114 (4), 137 (7), 112 (3)	118 (6)	Rat, Mouse, Marmoset
M_1	74	65	52	109	61	132	206	118 (2), 128 (12), 119 (7), 113 (8), 101 (3)	74 (2), 67 (12), 104 (3)	65 (2), 94 (12), 71 (7), 70 (8), 97 (3)	109 (2), 139 (12), 110 (7), 117 (8), 99 (3)	111(12)	Rat, Mouse, Marmoset
M_2	99	89	69	79	46	127	190	115 (2), 141 (12), 91 (7), 124 (8), 103 (3)	101 (2), 86 (12), 110 (3)	105 (2), 104 (12), 142 (7), 79 (8), 111 (3)	86 (2), 89 (12), 74 (7), 97 (8), 88 (3)	146 (12)	Rat, Mouse, Marmoset
nACh	83	126	80	131	91	109	80	56 (12), 103 (7),	56 (12)	56 (12), 45 (7)	260 (12), 152 (7)	185 (12)	Rat, Mouse
α_1	156	206	161	33	15	61	67	95 (2), 108 (7), 88 (3)	102 (2), 101 (3)	101 (2), 104 (7), 95 (3)	103 (2), 88 (7), 110 (3)	104 (13)	Rat, Mouse, Marmoset
α_2	92	68	75	150	52	142	120	103 (2)	90 (2)	86 (2)	105 (2)	132 (13)	Rat
$5\text{-}HT_{1A}$	130	100	93	87	101	97	93	93 (2), 79 (9), 205 (7)	44 (2)	73 (2), 29 (7)	130 (2), 119 (9), 66 (7)	27 (13)	Rat, Mouse
$D_{1/5}$	96	89	87	98	72	110	148	39 (2), 76 (10)	58 (2)	54 (2)	177 (2), 147 (10)	170 (11)	Rat

[1]Values for each structure correspond to the receptor density in percentage relative to the mean density of the receptor type in the hippocampus (mammals) or the HF (pigeons). The conclusion of this summary is illustrated in Figure 9. (1) Palomero-Gallagher et al., 2003; (2) Topic et al., 2007; (3) Kraemer et al., 1995; (4) Zilles et al., 2000; (5) Martens et al., 1998; (6) Cremer et al., 2009; (7) Cremer et al., 2011; (8) Wolff et al., 2008; (9) Zavitsanou et al., 2010; (10) Savosta et al., 1986; (11) Cremer et al., 2010; (12) Sihver et al., 1997; (13) our unpublished data.

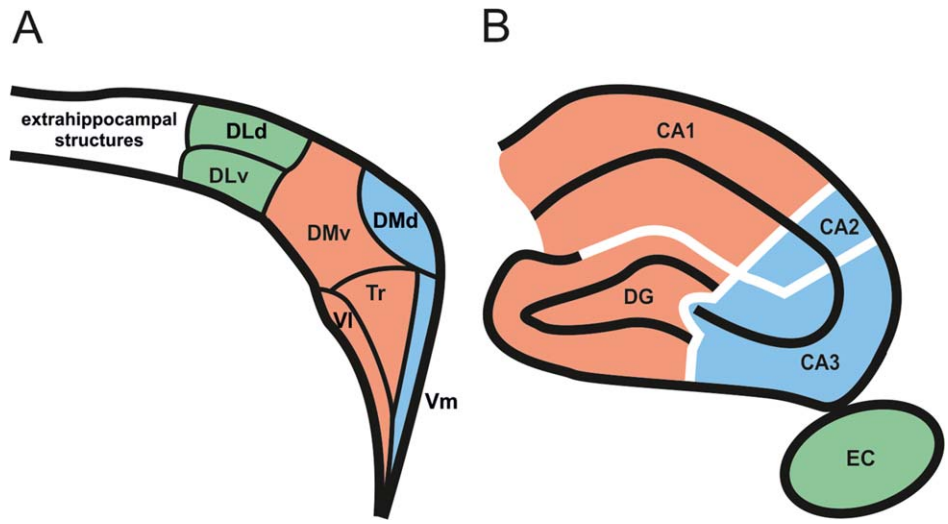

Figure 9. Similarities between receptor distribution in the subdivisions of the pigeon HF (**A**) and receptor distribution in the subdivisions of a typical (idealistic) mammalian hippocampus (**B**). The same colors indicate substantial overlap in relative receptor densities based on semiquantitative comparisons between the pigeon HF and the rat hippocampus (Table 2). Here DMv, Vl, and Tr share similarities with DG and CA1 (indicated in orange), and DMd and Vm share similarities with CA2 and CA3 (indicated in blue), whereas DLd/DLv share similarities with entorhinal cortex (EC; indicated in green). CA1, cornu ammonis field 1; CA2, cornu ammonis field 2; CA3, cornu ammonis field 3; DG, dentate gyrus; DMd, dorsal part of the dorsomedial region of HF; DMv, ventral part of the dorsomedial region of HF; DLd, dorsal part of dorsolateral region of HF; DLv, ventral part of dorsolateral region of HF; EC, entorhinal cortex; Tr, triangular region of the ventromedial region of HF; Vm, ventromedial part of the V-complex; Vl, ventrolateral part of the V-complex.

organization of mossy fibers in rats (Danscher et al., 1973; Danscher and Zimmer, 1978; Zimmer and Haug, 1978). At first glance, our findings also call into question whether mossy fibers, and by inference a strict equivalent to the DG, is present in birds, despite the indicators of our autoradiographic analysis. However, a further examination of Figure 8 shows that the V-complex of the avian HF is densely labeled with zinc, whereas in the DMv area staining is low, and the DMd is almost devoid of zinc staining. In the DL region, high levels of zinc could be observed in the DLv region but not in the DLd. No distinctive laminar-like labeling similar to the rat hippocampus could be observed. In fact, the diffuse but dense labeling in our V-complex resembles the diffuse and dense labeling in the CA regions of the primate hippocampus (Amaral et al., 2007). Therefore, if one considers the density of zinc labeling rather than looking for distinct mossy fibers, our V-complex resembles more the CA regions of mammals and particularly primates. On the other hand, not only the mossy fibers in the mammalian hippocampus are labeled with zinc. Zinc labeling occurred also in the granular cell layer and the molecular layer of DG (Zimmer and Haug, 1978; De Biasi and Bendotti, 1998). Given this fact, our zinc results do not exclude a correspondence between Vl/Tr and DG or Vm/DMv/DMd and the CA regions as suggested by the receptor data. Dense zinc labeling in the DLv and low labeling in DLd is in line with the nonhomogeneous labeling of EC and subiculum in the rat HF (Zimmer and Haug, 1978; Riba-Bosch and Perez-Clausell, 2004).

The colocalization of NMDA receptors and zinc characterizes much of Ammon's horn of the mammalian hippocampus, where glutamate and zinc (Zn^{2+}) are coreleased (Sindreu et al., 2003; Qian and Noebels, 2005). Thus, the extent to which NMDA receptors and zinc colocalize in the avian HF is of additional comparative interest. However, one limitation of our staining technique is that it labeled only vesicular zinc, leaving extracellular zinc undetected. Despite this limitation, examination of the NMDA fingerprint in Figure 5 and the zinc labeling in Figure 8 reveals some notable similarities. Based on the fingerprints, the highest density of NMDA receptors were found in Vl and Tr of the V-complex, where there was also dense labeling for zinc. Vm, by contrast, had lower NMDA receptor densities and less dense zinc labeling. Similarities continue in the two DM subdivisions, where higher NMDA and zinc labeling densities were found in DMv compared with DMd. Overall, there is an apparent correlation between the density of NMDA receptors and the zinc labeling density in the avian HF, a pattern also found in the mammalian hippocampus. From the perspective of possible subdivision parallels, the dense coupling of NMDA

receptors and zinc in Vl and Tr argues for similarity with the CA fields of Ammon's horn.

CONCLUSIONS

Although the mammalian hippocampus and avian HF derive from the same portion of the developing pallium (Reiner et al., 2004; Jarvis et al., 2013), their relationship to the rest of the forebrain is somewhat different. Whereas the mammalian hippocampus interacts, indirectly, with virtually the entire neocortex (Bird and Burgess, 2008), the avian HF has more limited connectivity (Csillag et al., 1994; Leutgeb et al., 1996; Kröner and Güntürkün, 1999; Atoji et al., 2002; Atoji and Wild, 2005). For example, unlike the case for the mammalian hippocampus, only a small projection from the medial septum to HF has been detected (Casini et al., 1986; Atoji and Wild, 2004; Montagnese et al., 2004). Given the incomplete correspondence in the subdivisional organization of the mammalian and avian HF, it is tempting to speculate that the differences in connectivity can in part explain how the two systems evolved different internal characteristics (Aboitiz, 1993; Manns and Eichenbaum, 2005; Papp et al., 2007; Rattenborg and Martinez-Gonzalez, 2011). However, in both mammals and birds, the hippocampal formation shares a number of morphological, physiological, and neurochemical similarities (Krebs et al., 1989; Bingman and Mench, 1990; Erichsen et al., 1991; Montagnese et al., 1993; Colombo et al., 1997; Margrie et al., 1998; Gagliardo et al., 1999; Tömböl et al., 2000a; Atoji et al., 2002; Budzynski et al., 2002; Bingman et al., 2003, 2005; Kahn et al., 2003; Atoji and Wild, 2004, 2005, 2006; Hough and Bingman, 2004; Bischof et al., 2006; Nair-Roberts et al., 2006; Hoshooley and Sherry, 2007; Sherry, 2011; Gupta et al., 2012) and plays a similar role in cognition, especially in spatial cognition (Bingman et al., 1998; Colombo and Broadbent, 2000; Suzuki and Clayton, 2000; Tommasi et al., 2003; Watanabe and Bischof, 2004; Ruploh et al., 2011; Mayer et al., 2012). By comparing the receptor architectonic profile of the pigeon HF with the mammalian hippocampus, we detected a number of shared traits (Fig. 9). However, as indicated by a study in the zebra finch that investigated the expression of immediate early genes during spatial learning, a study that detected individual patch locations that were not in line with previously described hippocampal subdivisions (Mayer et al., 2012), it may be possible that information processing in the HF of birds is, at least in part, different from that in the mammalian hippocampus (but see Kahn et al., 2003). Székély (1999) also came to the same conclusion, that the avian HF probably has a somewhat different wiring organization compared with the mammalian hippocampus. Therefore, in assuming a kind of nonlaminar, network organization for the avian HF (for review see Atoji and Wild, 2006), it may be that there was less selective pressure to organize the avian HF into anatomically discrete subdivisions such as those found in the mammalian hippocampus. Another point is that, although the avian HF and mammalian hippocampus develop from the same type of cells during development, so far expression profiles of selective markers have not clarified whether these cells are more amygdala- or more cortex-like, or both (Reiner et al., 2004; Dugas-Ford et al., 2012; Chen et al., 2013; Jarvis et al., 2013). To understand the development of hippocampal subfields, it is also very important to understand how cells originate, how cells migrate, and during which time window cells express specific genes that organize their future targets during development (Christie et al., 2013; Montiel and Molnar, 2013). As one last consideration, from analysis of gene expression profiles between different species, some researchers have proposed that the DG is one of the most recently evolved structures of the mammalian brain (see Kempermann, 2012). Thus, it may be that birds did not evolve a DG, but this would not exclude the independent evolution of a functional equivalent, as has been shown for the nidopallium caudolaterale of birds and the prefrontal cortex of mammals (Güntürkün, 2012).

Overall, our study reveals an avian HF characterized by distinct subdivisions based on differences in receptor-type distribution and zinc density. Similarities to the mammalian HF could be observed between Vl/Tr/DMv and DG/CA1, between Vm/DMd and CA2/CA3, and between DL and Ent (Table 2, Fig. 9). However, we suggest that 300 hundred million years of independent evolution has led to a mosaic of similarities and differences in the subdivisional organization of the avian HF and mammalian hippocampus and that thinking about the avian HF in terms of the strict subdivisional organization of the mammalian hippocampus is likely insufficient to understand the avian HF.

CONFLICT OF INTEREST STATEMENT

The authors declare that there are no conflicts of interest.

ROLE OF AUTHORS

All authors had full access to all the data in the study and take responsibility for the integrity of the data and the accuracy of the data analysis. Study concept and design: CH, VPB, KZ, OG. Acquisition of data: CH, NP-G, SL, FS. Analysis and interpretation of data:

CH, VPB, MS, OG. Drafting of the manuscript: CH, VPB, OG. Critical revision of the manuscript for important intellectual content: CH, VPB, MS, KZ, OG. Statistical analysis: CH. Obtained funding: VPB, Z, OG. Administrative, technical, and material support: CH, NP-G, SL, FS. Study supervision: CH, NP-G, KZ, OG.

LITERATURE CITED

Aboitiz F. 1993. Further comments on the evolutionary origin of the mammalian brain. Med Hypoth 41:409–418.

Altman J. 1962. Are new neurons formed in the brains of adult mammals? Science 135:1127–1128.

Amaral DG, Witter MP. 1989. The three-dimensional organization of the hippocampal formation: a review of anatomical data. Neuroscience 31:571–591.

Amaral DG, Scharfman HE, Lavenex P. 2007. The dentate gyrus: fundamental neuroanatomical organization (dentate gyrus for dummies). Prog Brain Res 163:3–22.

Amunts K, Kedo O, Kindler M, Pieperhoff P, Mohlberg H, Shah NJ, Habel U, Schneider F, Zilles K. 2005. Cytoarchitectonic mapping of the human amygdala, hippocampal region and entorhinal cortex: intersubject variability and probability maps. Anat Embryol 210:343–352.

Atoji Y, Wild JM. 2004. Fiber connections of the hippocampal formation and septum and subdivisions of the hippocampal formation in the pigeon as revealed by tract tracing and kainic acid lesions. J Comp Neurol 475:426–461.

Atoji Y, Wild JM. 2005. Afferent and efferent connections of the dorsolateral corticoid area and a comparison with connections of the temporo-parieto-occipital area in the pigeon (*Columba livia*). J Comp Neurol 485:165–182.

Atoji Y, Wild JM. 2006. Anatomy of the avian hippocampal formation. Rev Neurosci 17:3–15.

Atoji Y, Wild JM, Yamamoto Y, Suzuki Y. 2002. Intratelencephalic connections of the hippocampus in pigeons (*Columba livia*). J Comp Neurol 447:177–199.

Ball GF, Nock B, Wingfield JC, McEwen BS, Balthazart J. 1990. Muscarinic cholinergic receptors in the songbird and quail brain: a quantitative autoradiographic study. J Comp Neurol 298:431–442.

Ball GF, Casto JM, Balthazart J. 1995. Autoradiographic localization of D1-like dopamine receptors in the forebrain of male and female Japanese quail and their relationship with immunoreactive tyrosine hydroxylase. J Chem Neuroanat 9:121–133.

Barnea A, Nottebohm F. 1994. Seasonal recruitment of hippocampal neurons in adult free-ranging black-capped chickadees. Proc Natl Acad Sci U S A 91:11217–11221.

Bingman VP, Mench JA. 1990. Homing behavior of hippocampus and parahippocampus lesioned pigeons following short-distance releases. Behav Brain Res 40:227–238.

Bingman VP, Strasser R, Baker C, Riters LV. 1998. Paired-associate learning is unaffected by combined hippocampal and parahippocampal lesions in homing pigeons. Behav Neurosci 112:533–540.

Bingman VP, Hough GE 2nd, Kahn MC, Siegel JJ. 2003. The homing pigeon hippocampus and space: in search of adaptive specialization. Brain Behav Evol 62:117–127.

Bingman VP, Gagliardo A, Hough GE 2nd, Ioale P, Kahn MC, Siegel JJ. 2005. The avian hippocampus, homing in pigeons and the memory representation of large-scale space. Integr Comp Biol 45:555–564.

Bird CM, Burgess N. 2008. The hippocampus and memory: insights from spatial processing. Nat Rev Neurosci 9:182–194.

Bischof HJ, Lieshoff C, Watanabe S. 2006. Spatial memory and hippocampal function in a non-foodstoring songbird, the zebra finch (*Taeniopygia guttata*). Rev Neurosci 17: 43–52.

Budzynski CA, Gagliardo A, Ioale P, Bingman VP. 2002. Participation of the homing pigeon thalamofugal visual pathway in sun-compass associative learning. Eur J Neurosci 15:197–210.

Casini G, Bingman VP, Bagnoli P. 1986. Connections of the pigeon dorsomedial forebrain studied with WGA-HRP and ^{3}H-proline. J Comp Neurol 245:454–470.

Chen CC, Winkler CM, Pfenning AR, Jarvis ED. 2013. Molecular profiling of the developing avian telencephalon: regional timing and brain subdivision continuities. J Comp Neurol 521:3666–3701.

Christie KJ, Emery B, Denham M, Bujalka H, Cate HS, Turnley AM. 2013. Transcriptional regulation and specification of neural stem cells. Adv Exp Med Biol 786:129–155.

Colombo M, Broadbent N. 2000. Is the avian hippocampus a functional homologue of the mammalian hippocampus? Neurosci Biobehav Rev 24:465–484.

Colombo M, Cawley S, Broadbent N. 1997. The effects of hippocampal and area parahippocampalis lesions in pigeons: II. Concurrent discrimination and spatial memory. Q J Exp Psychol B 50:172–189.

Craigie EH. 1930. Studies on the brain of the kiwi (*Apteryx australis*). J Comp Neurol 49:223–357.

Craigie EH. 1935. The cerebral hemispheres of the kiwi and of the emu (*Apteryx* and *Dromiceius*). J Anat 69:380–393.

Cremer CM, Palomero-Gallagher N, Bidmon HJ, Schleicher A, Speckmann EJ, Zilles K. 2009. Pentylenetetrazole-induced seizures affect binding site densities for GABA, glutamate and adenosine receptors in the rat brain. Neuroscience 163:490–499.

Cremer CM, Bidmon HJ, Gorg B, Palomero-Gallagher N, Escobar JL, Speckmann EJ, Zilles K. 2010. Inhibition of glutamate/glutamine cycle in vivo results in decreased benzodiazepine binding and differentially regulated GABAergic subunit expression in the rat brain. Epilepsia 51:1446–1455.

Cremer CM, Lubke JH, Palomero-Gallagher N, Zilles K. 2011. Laminar distribution of neurotransmitter receptors in different reeler mouse brain regions. Brain Struct Funct 216:201–218.

Csillag A, Székély AD, Davies DC. 1994. Termination pattern of medial hyperstriatum ventrale efferents in the archistriatum of the domestic chick. J Comp Neurol 348:394–402.

Danscher G, Zimmer J. 1978. An improved Timm sulphide silver method for light and electron microscopic localization of heavy metals in biological tissues. Histochemistry 55:27–40.

Danscher G, Haug FM, Fredens K. 1973. Effect of diethyldithiocarbamate (DEDTC) on sulphide silver stained boutons. Reversible blocking of Timm's sulphide silver stain for "heavy" metals in DEDTC treated rats (light microscopy). Exp Brain Res 16:521–532.

De Biasi S, Bendotti C. 1998. A simplified procedure for the physical development of the sulphide silver method to reveal synaptic zinc in combination with immunocytochemistry at light and electron microscopy. J Neurosci Methods 79:87–96.

Dietl MM, Palacios JM. 1988. Neurotransmitter receptors in the avian brain. I. Dopamine receptors. Brain Res 439: 354–359.

Dietl MM, Cortes R, Palacios JM. 1988. Neurotransmitter receptors in the avian brain. II. Muscarinic cholinergic receptors. Brain Res 439:360–365.

Dugas-Ford J, Rowell JJ, Ragsdale CW. 2012. Cell-type homologies and the origins of the neocortex. Proc Natl Acad Sci U S A 109:16974–16979.

Erichsen JT, Bingman VP, Krebs JR. 1991. The distribution of neuropeptides in the dorsomedial telencephalon of the pigeon (*Columba livia*): a basis for regional subdivisions. J Comp Neurol 314:478–492.

Eriksson PS, Perfilieva E, Bjork-Eriksson T, Alborn AM, Nordborg C, Peterson DA, Gage FH. 1998. Neurogenesis in the adult human hippocampus. Nat Med 4:1313–1317.

Faber H, Braun K, Zuschratter W, Scheich H. 1989. System-specific distribution of zinc in the chick brain. A light- and electron-microscopic study using the Timm method. Cell Tissue Res 258:247–257.

Gagliardo A, Ioale P, Bingman VP. 1999. Homing in pigeons: the role of the hippocampal formation in the representation of landmarks used for navigation. J Neurosci 19: 311–315.

Güntürkün O. 2012. The convergent evolution of neural substrates for cognition. Psychol Res 76:212–219.

Gupta S, Maurya R, Saxena M, Sen J. 2012. Defining structural homology between the mammalian and avian hippocampus through conserved gene expression patterns observed in the chick embryo. Dev Biol 366:125–141.

Heimovics SA, Cornil CA, Ellis JM, Ball GF, Riters LV. 2011. Seasonal and individual variation in singing behavior correlates with alpha2-noradrenergic receptor density in brain regions implicated in song, sexual, and social behavior. Neuroscience 182:133–143.

Herold C, Palomero-Gallagher N, Hellmann B, Kröner S, Theiss C, Güntürkün O, Zilles K. 2011. The receptor architecture of the pigeons' nidopallium caudolaterale: an avian analogue to the mammalian prefrontal cortex. Brain Struct Funct 216:239–254.

Herold C, Palomero-Gallagher N, Güntürkün O, Zilles K. 2012. Serotonin 5-HT_{1A} receptor binding sites in the brain of the pigeon (*Columba livia*). Neuroscience 200:1–12.

Hoshooley JS, Sherry DF. 2007. Greater hippocampal neuronal recruitment in food-storing than in non-food-storing birds. Dev Neurobiol 67:406–414.

Hoshooley JS, Phillmore LS, Macdougall-Shackleton SA. 2005. An examination of avian hippocampal neurogenesis in relationship to photoperiod. Neuroreport 16:987–991.

Hough GE, Bingman VP. 2004. Spatial response properties of homing pigeon hippocampal neurons: correlations with goal locations, movement between goals, and environmental context in a radial-arm arena. J Comp Physiol A Neuroethol Sens Neural Behav Physiol 190:1047–1062.

Insausti R. 1993. Comparative anatomy of the entorhinal cortex and hippocampus in mammals. Hippocampus 3(Spec No.):19–26.

Jarvis ED, Yu J, Rivas MV, Horita H, Feenders G, Whitney O, Jarvis SC, Jarvis ER, Kubikova L, Puck AE, Siang-Bakshi C, Martin S, McElroy M, Hara E, Howard J, Pfenning A, Mouritsen H, Chen CC, Wada K. 2013. Global view of the functional molecular organization of the avian cerebrum: mirror images and functional columns. J Comp Neurol 521:Spc1.

Kahn MC, Hough GE 2nd, Ten Eyck GR, Bingman VP. 2003. Internal connectivity of the homing pigeon (*Columba livia*) hippocampal formation: an anterograde and retrograde tracer study. J Comp Neurol 459:127–141.

Kallen B. 1962. II. Embryogenesis of brain nuclei in the chick telencephalon. Ergeb Anat Entwicklungsgesch 36:62–82.

Karten H, Hodos W. 1967. A stereotaxic atlas of the brain of the pigeon (*Columba livia*). Baltimore: The Johns Hopkins University Press.

Kempermann G. 2012. New neurons for "survival of the fittest." Nat Rev Neurosci 13:727–736.

Kleitz HK, Cornil CA, Balthazart J, Ball GF. 2009. Species differences in the relative densities of D1- and D2-like dopamine receptor subtypes in the Japanese quail and rats: an in vitro quantitative receptor autoradiography study. Brain Behav Evol 73:81–90.

Kraemer M, Zilles K, Schleicher A, Gebhard R, Robbins TW, Everitt BJ, Divac I. 1995. Quantitative receptor autoradiography of eight different transmitter-binding sites in the hippocampus of the common marmoset, *Callithrix jacchus*. Anat Embryol 191:213–225.

Krebs JR, Sherry DF, Healy SD, Perry VH, Vaccarino AL. 1989. Hippocampal specialization of food-storing birds. Proc Natl Acad Sci U S A 86:1388–1392.

Krebs JR, Erichsen JT, Bingman VP. 1991. The distribution of neurotransmitters and neurotransmitter-related enzymes in the dorsomedial telencephalon of the pigeon (*Columba livia*). J Comp Neurol 314:467–477.

Kröner S, Güntürkün O. 1999. Afferent and efferent connections of the caudolateral neostriatum in the pigeon (*Columba livia*): a retro- and anterograde pathway tracing study. J Comp Neurol 407:228–260.

Leutgeb S, Husband S, Riters LV, Shimizu T, Bingman VP. 1996. Telencephalic afferents to the caudolateral neostriatum of the pigeon. Brain Res 730:173–181.

Manns JR, Eichenbaum H. 2005. Time and treason to the trisynaptic teachings: theoretical comment on Kesner et al. (2005). Behav Neurosci 119:1140–1143.

Margrie TW, Rostas JA, Sah P. 1998. Long-term potentiation of synaptic transmission in the avian hippocampus. J Neurosci 18:1207–1216.

Mayer U, Watanabe S, Bischof HJ. 2009. Hippocampal activation of immediate early genes Zenk and c-Fos in zebra finches (*Taeniopygia guttata*) during learning and recall of a spatial memory task. Neurobiol Learn Mem 93:322–329.

Mayer U, Watanabe S, Bischof HJ. 2012. Spatial memory and the avian hippocampus: research in zebra finches. J Physiol Paris doi: 10.1016/j.jphysparis.2012.05.002.

Merker B. 1983. Silver staining of cell bodies by means of physical development. J Neurosci Methods 9:235–241.

Ming GL, Song H. 2005. Adult neurogenesis in the mammalian central nervous system. Annu Rev Neurosci 28:223–250.

Molla R, Rodriguez J, Calvet S, Garcia-Verdugo JM. 1986. Neuronal types of the cerebral cortex of the adult chicken (*Gallus gallus*). A Golgi study. J Hirnforsch 27:381–390.

Montagnese CM, Geneser FA, Krebs JR. 1993. Histochemical distribution of zinc in the brain of the zebra finch (*Taenopygia guttata*). Anat Embryol 188:173–187.

Montagnese CM, Krebs JR, Meyer G. 1996. The dorsomedial and dorsolateral forebrain of the zebra finch, *Taeniopygia guttata*: a Golgi study. Cell Tissue Res 283:263–282.

Montagnese CM, Székély AD, Adam A, Csillag A. 2004. Efferent connections of septal nuclei of the domestic chick (*Gallus domesticus*): an anterograde pathway tracing study with a bearing on functional circuits. J Comp Neurol 469:437–456.

Montiel JF, Molnar Z. 2013. The impact of gene expression analysis on evolving views of avian brain organization. J Comp Neurol 521:3604–3613.

Nair-Roberts RG, Erichsen JT, Reboreda JC, Kacelnik A. 2006. Distribution of substance P reveals a novel subdivision in the hippocampus of parasitic South American cowbirds. J Comp Neurol 496:610–626.

Palomero-Gallagher N. 1999. Transmitterrezeptoren im Hippocampus verschiedener Säugetiere: Vergleichend-anatomische Untersuchungen und Analyse geschlechts-

und zyklusabhängiger Verteilungsmuster. Dissertation, Heinrich-Heine-Universität Düsseldorf.

Palomero-Gallagher N, Bidmon HJ, Zilles K. 2003. AMPA, kainate, and NMDA receptor densities in the hippocampus of untreated male rats and females in estrus and diestrus. J Comp Neurol 459:468–474.

Palomero-Gallagher N, Schleicher A, Lindemann S, Lessenich A, Zilles K, Loscher W. 2008. Receptor fingerprinting the circling ci2 rat mutant: insights into brain asymmetry and motor control. Exp Neurol 210:624–637.

Papp G, Witter MP, Treves A. 2007. The CA3 network as a memory store for spatial representations. Learn Mem 14:732–744.

Pauly JR, Stitzel JA, Marks MJ, Collins AC. 1989. An autoradiographic analysis of cholinergic receptors in mouse brain. Brain Res Bull 22:453–459.

Puelles L, Martinez-de-la-Torre M, Paxinos G, Watson C, Martinez S. 2007. The chick brain in stereotaxic coordinates: an atlas featuring neuromeric subdivisions and mammalian homologies. San Diego: Acadamic Press.

Pytte CL, Gerson M, Miller J, Kirn JR. 2007. Increasing stereotypy in adult zebra finch song correlates with a declining rate of adult neurogenesis. Dev Neurobiol 67:1699–1720.

Qian J, Noebels JL. 2005. Visualization of transmitter release with zinc fluorescence detection at the mouse hippocampal mossy fibre synapse. J Physiol 566:747–758.

Rattenborg NC, Martinez-Gonzalez D. 2011. A bird-brain view of episodic memory. Behav Brain Res 222:236–245.

Reiner A, Perkel DJ, Bruce LL, Butler AB, Csillag A, Kuenzel W, Medina L, Paxinos G, Shimizu T, Striedter G, Wild M, Ball GF, Durand S, Gunturkun O, Lee DW, Mello CV, Powers A, White SA, Hough G, Kubikova L, Smulders TV, Wada K, Dugas-Ford J, Husband S, Yamamoto K, Yu J, Siang C, Jarvis ED, Avian Brain Nomenclature F. 2004. Revised nomenclature for avian telencephalon and some related brainstem nuclei. J Comp Neurol 473:377–414.

Riba-Bosch A, Perez-Clausell J. 2004. Response to kainic acid injections: changes in staining for zinc, FOS, cell death and glial response in the rat forebrain. Neuroscience 125:803–818.

Rodriguez F, Lopez JC, Vargas JP, Broglio C, Gomez Y, Salas C. 2002. Spatial memory and hippocampal pallium through vertebrate evolution: insights from reptiles and teleost fish. Brain Res Bull 57:499–503.

Rose M. 1912. Histologische Lokalisation der Großhirnrinde bei kleinen Säugetieren. J Psychol Neurol 19.

Rose M. 1914. Über die cytoarchitektonische Gleiderung des Vorderhinrs der Vögel. J Psychol Neurol 21:278–352.

Rose M. 1926. Der Allocortex bei Tier und Mensch 1. Teil. Jour Psychol Neurol 34:1–111.

Rosinha MU, Ferrari EA, Toledo CA. 2009. Immunohistochemical distribution of AMPA-type label in the pigeon (*C. livia*) hippocampus. Neuroscience 159:438–450.

Ruploh T, Kazek A, Bischof HJ. 2011. Spatial orientation in Japanese quails (*Coturnix coturnix japonica*). PLoS One 6: e28202.

Schleicher A, Palomero-Gallagher N, Morosan P, Eickhoff SB, Kowalski T, de Vos K, Amunts K, Zilles K. 2005. Quantitative architectural analysis: a new approach to cortical mapping. Anat Embryol 210:373–386.

Schnabel R, Braun K. 1996. Development of dopamine receptors in the forebrain of the domestic chick in relation to auditory imprinting. An autoradiographic study. Brain Res 720:120–130.

Sherry DF. 2011. The hippocampus of food-storing birds. Brain Behav Evol 78:133–135.

Sherry DF, Jacobs LF, Gaulin SJ. 1992. Spatial memory and adaptive specialization of the hippocampus. Trends Neurosci 15:298–303.

Siegel JJ, Nitz D, Bingman VP. 2000. Hippocampal theta rhythm in awake, freely moving homing pigeons. Hippocampus 10:627–631.

Siegel JJ, Nitz D, Bingman VP. 2002. Electrophysiological profile of avian hippocampal unit activity: a basis for regional subdivisions. J Comp Neurol 445:256–268.

Sihver W, Günther P, Schiebs R, Bigl V. 1997. Repeated administration of tacrine to normal rats: effects on cholinergic, glutamamtergic and gabaergic receptor subtypes in rat using receptor autoradiography. Neurochem Int 31: 693–703.

Sindreu CB, Varoqui H, Erickson JD, Perez-Clausell J. 2003. Boutons containing vesicular zinc define a subpopulation of synapses with low AMPAR content in rat hippocampus. Cereb Cortex 13:823–829.

Stewart MG, Cristol D, Philips R, Steele RJ, Stamatakis A, Harrison E, Clayton N. 1999. A quantitative autoradiographic comparison of binding to glutamate receptor sub-types in hippocampus and forebrain regions of a food-storing and a non-food-storing bird. Behav Brain Res 98:89–94.

Suarez J, Davila JC, Real MA, Guirado S, Medina L. 2006. Calcium-binding proteins, neuronal nitric oxide synthase, and GABA help to distinguish different pallial areas in the developing and adult chicken. I. Hippocampal formation and hyperpallium. J Comp Neurol 497:751–771.

Suzuki WA, Clayton NS. 2000. The hippocampus and memory: a comparative and ethological perspective. Curr Opin Neurobiol 10:768–773.

Székély AD. 1999. The avian hippocampal formation: subdivisions and connectivity. Behav Brain Res 98:219–225.

Székély AD, Krebs JR. 1996. Efferent connectivity of the hippocampal formation of the zebra finch (*Taenopygia guttata*): an anterograde pathway tracing study using *Phaseolus vulgaris* leucoagglutinin. J Comp Neurol 368: 198–214.

Tömböl T, Davies DC, Nemeth A, Alpar A, Sebesteny T. 2000a. A golgi and a combined Golgi/GABA immunogold study of local circuit neurons in the homing pigeon hippocampus. Anat Embryol 201:181–196.

Tömböl T, Davies DC, Nemeth A, Sebesteny T, Alpar A. 2000b. A comparative Golgi study of chicken (*Gallus domesticus*) and homing pigeon (*Columba livia*) hippocampus. Anat Embryol 201:85–101.

Tommasi L, Gagliardo A, Andrew RJ, Vallortigara G. 2003. Separate processing mechanisms for encoding of geometric and landmark information in the avian hippocampus. Eur J Neurosci 17:1695–1702.

Topic B, Willuhn I, Palomero-Gallagher N, Zilles K, Huston JP, Hasenohrl RU. 2007. Impaired maze performance in aged rats is accompanied by increased density of NMDA, 5-HT_{1A}, and alpha-adrenoceptor binding in hippocampus. Hippocampus 17:68–77.

Veenman CL, Albin RL, Richfield EK, Reiner A. 1994. Distributions of $GABA_A$, GABAB, and benzodiazepine receptors in the forebrain and midbrain of pigeons. J Comp Neurol 344:161–189.

Watanabe S, Bischof HJ. 2004. Effects of hippocampal lesions on acquisition and retention of spatial learning in zebra finches. Behav Brain Res 155:147–152.

Witter MP. 2007. Intrinsic and extrinsic wiring of CA3: indications for connectional heterogeneity. Learn Mem 14: 705–713.

Wolff SC, Hruska Z, Nguyen L, Dohanich GP. 2008. Asymmetrical distributions of muscarinic receptor binding in the

hippocampus of female rats. Eur J Pharmacol 588:248–250.

Zilles K, Qu M, Schleicher A. 1993. Regional distribution and heterogeneity of alpha-adrenoceptors in the rat and human central nervous system. J Hirnforsch 34:123–132.

Zilles K, Wu J, Crusio WE, Schwegler H. 2000. Water maze and radial maze learning and the density of binding sites of glutamate, GABA, and serotonin receptors in the hippocampus of inbred mouse strains. Hippocampus 10: 213–225.

Zilles K, Palomero-Gallagher N, Grefkes C, Scheperjans F, Boy C, Amunts K, Schleicher A. 2002a. Architectonics of the human cerebral cortex and transmitter receptor fingerprints: reconciling functional neuroanatomy and neurochemistry. Eur Neuropsychopharmacol 12:587–599.

Zilles K, Schleicher A, Palomero-Gallagher N, Amunts K. 2002b. Quantitative analysis of cyto- and receptor architecture of the human brain. In: Mazziotta JC, Toga A, editors. Brain mapping: the methods. Amsterdam: Elsevier. p 573–602.

Zimmer J, Haug FM. 1978. Laminar differentiation of the hippocampus, fascia dentata and subiculum in developing rats, observed with the Timm sulphide silver method. J Comp Neurol 179:581–617.